

Coupled Markov chain Monte Carlo for high-dimensional regression with Half-t priors

Niloy Biswas ^{*} Anirban Bhattacharya [†] Pierre E. Jacob [‡] James E. Johndrow [§]

October 6, 2021

Abstract

Continuous shrinkage priors are commonly used in Bayesian analysis of high-dimensional data, due to both their computational advantages and favorable statistical properties. We develop coupled Markov chain Monte Carlo (MCMC) algorithms for Bayesian shrinkage regression in high dimensions. Following Glynn & Rhee (2014), these couplings can be used in parallel computation strategies and practical diagnostics of convergence. Focusing on a class of shrinkage priors which includes the Horseshoe, we demonstrate the scalability of the proposed couplings with data from a genome-wide association study with 2000 rows and 100,000 covariates. The results highlight the impact of the shrinkage prior on the computational efficiency of the coupling procedure, and motivate priors where the local precisions are Half-t distributed with degree of freedom larger than one, which are statistically justifiable in terms of posterior concentration, and lead to practical computations.

1 Introduction

1.1 Bayesian computation in high dimensions

We consider the setting of high-dimensional regression where the number of observations n is smaller than the number of covariates p and the true signal is sparse. This problem formulation is ubiquitous in modern applications ranging from genomics to the social sciences. Optimization-based methods allow sparse point estimates, such as the LASSO [Tibshirani, 1994] or Elastic Net [Zou and Hastie, 2005], to be obtained even when the number of covariates is on the order of hundreds of thousands. More specifically, iterative optimization procedures to obtain these estimates are practical because the following conditions are met: 1) the cost per iteration scales favorably with the size of the input (n and p), 2) the number of iterations to convergence also scales favorably with the size of the input, and 3) there are reliable stopping criteria to detect convergence.

In the Bayesian paradigm, Markov chain Monte Carlo (MCMC) methods are commonly used to sample from the posterior distribution. A naïve application of MCMC algorithms to high-dimensional settings can lead to high computational costs, both per iteration and in terms of the number of iterations to reach convergence, but tailored algorithms can provide substantial improvements. Stopping criteria for MCMC have been proposed in various forms, such as univariate effective sample size [ESS, e.g Vats et al., 2019], or the \hat{R} convergence diagnostic [e.g. Vats and Knudson, 2020], but the question of convergence diagnostics remains mostly open. The aforementioned diagnostics rely on the asymptotic behavior of the chains as time goes to infinity. The lack of non-asymptotic stopping criteria poses an important practical problem. With Bayesian computation in high-dimensional settings, the specification of the prior, the size of the data set and the signal-to-noise ratio in the data all impact the performance of MCMC algorithms. Since these factors vary across applications, practitioners face difficulties when choosing the number of iterations to run and the proportion of initial iterations to discard as “burn-in”. This could lead users to either waste computational

^{*}Department of Statistics, Harvard University. Email: niloy_biswas@g.harvard.edu

[†]Department of Statistics, Texas A&M University. Email: anirbanb@stat.tamu.edu

[‡]Department of Statistics, Harvard University. Email: pjacob@fas.harvard.edu

[§]Department of Statistics, The Wharton School, University of Pennsylvania. Email: johndrow@wharton.upenn.edu

resources by running overly long chains, or, conversely, to base their analysis on chains that have not converged. This manuscript proposes a concrete method to avoid these pitfalls in the case of a Gibbs sampler for Bayesian regression with shrinkage priors. Specifically, we use couplings to construct stopping criteria and determine burn-in size in an effort to reduce the gap between MCMC-based and optimization-based computation for high-dimensional regression.

1.2 Bayesian shrinkage regression with Half- $t(\nu)$ priors

Consider Gaussian linear regression with n observations and p covariates, with a focus on the high-dimensional setting where $n \ll p$. The likelihood is given by

$$L(\beta, \sigma^2; X, y) = \frac{1}{(2\pi\sigma^2)^{n/2}} \exp\left(-\frac{1}{2\sigma^2}\|y - X\beta\|^2\right), \quad (1)$$

where $\|\cdot\|$ denotes the L_2 norm, $X \in \mathbb{R}^{n \times p}$ is the observed design matrix, $y \in \mathbb{R}^n$ is the observed response vector, $\sigma^2 > 0$ is the unknown Gaussian noise variance, and $\beta \in \mathbb{R}^p$ is the unknown signal vector that is assumed to be sparse. Consider a hierarchical Gaussian scale-mixture prior on (β, σ^2) , given by

$$\beta_j \mid \sigma^2, \xi, \eta \underset{j=1, \dots, p}{\stackrel{\text{ind}}{\sim}} \mathcal{N}\left(0, \frac{\sigma^2}{\xi\eta_j}\right), \quad \xi \sim \pi_\xi(\cdot), \quad \eta_j \underset{j=1, \dots, p}{\stackrel{\text{i.i.d.}}{\sim}} \pi_\eta(\cdot), \quad \sigma^2 \sim \text{InvGamma}\left(\frac{a_0}{2}, \frac{b_0}{2}\right), \quad (2)$$

where $a_0, b_0 > 0$, and $\pi_\xi(\cdot), \pi_\eta(\cdot)$ are continuous densities on $\mathbb{R}_{>0}$. Such global-local mixture priors induce approximate sparsity, where the components of β can be arbitrarily close to but never exactly equal zero. This is in contrast to point-mass mixture priors [e.g [Johnson and Rossell, 2012](#)], where some components of β can be exactly zero a posteriori. The global precision parameter ξ relates to the number of signals, and we use $\xi^{-1/2} \sim \text{Cauchy}_+(0, 1)$ throughout. The local precision parameters η_j determine which components of β are null.

We focus on the Half- $t(\nu)$ prior family for the local scale parameter, $\eta_j^{-1/2} \sim t_+(\nu)$ for $\nu \geq 1$, where a $t_+(\nu)$ distribution has density proportional to $(1 + x^2/\nu)^{-(\nu+1)/2} \mathbb{1}_{(0,\infty)}(x)$. The induced prior on the local precision η_j has density

$$\pi_\eta(\eta_j) \propto \frac{1}{\eta_j^{\frac{2-\nu}{2}} (1 + \nu\eta_j)^{\frac{\nu+1}{2}}} \mathbb{1}_{(0,\infty)}(\eta_j). \quad (3)$$

The case $\nu = 1$ corresponds to the Horseshoe prior [[Carvalho et al., 2009, 2010](#)] and has received overwhelming attention in the literature among this prior class; see [Bhadra et al. \[2019\]](#) for a recent overview. The usage of general Half- $t(\nu)$ priors on prior scale parameters in hierarchical Gaussian models dates back to [Gelman \[2006\]](#). However, the subsequent literature has largely gravitated towards the default choice [[Polson and Scott, 2012](#)] of $\nu = 1$, in part because a convincing argument for preferring a different value of ν has been absent to date. We discuss below that Half- $t(\nu)$ priors empirically yield statistical estimation properties as strong as the Horseshoe prior, whilst leading to significant computational gains when $\nu > 1$. While our evidence regarding the statistical performance is empirical in nature, we note that [Ghosh and Chakrabarti \[2017\]](#) established optimal posterior concentration in the Normal means problem for a broad class of priors on the local scale that includes the Half- $t(\nu)$ priors, extending earlier work by [van der Pas et al. \[2014\]](#) for the Horseshoe.

Our stopping criteria relies on couplings. Couplings have long been used to analyze the convergence of MCMC algorithms, while methodological implementations have been rare. The work of [Johnson \[1996, 1998\]](#) has pioneered the use of couplings for practical diagnostics of convergence, but relied on the assumption of some similarity between the initial distribution and the target, which can be hard to check. Here we instead follow the approach of [Glynn and Rhee \[2014\]](#), [Jacob et al. \[2020\]](#) based on couplings of lagged chains, applied to the question of convergence in [Biswas et al. \[2019\]](#). That approach makes no assumptions on the closeness of the initial distribution to the target, and in our experiments we initialize chains from the prior distribution.

The approach requires the ability to sample pairs of Markov chains such that 1) each chain marginally follows a prescribed MCMC algorithm and 2) the two chains “meet” after a random –but almost surely finite– number of iterations, called the meeting time. When the chains meet, i.e. when all of their components become identical, the user can stop the procedure. From the output the user can obtain unbiased estimates

of expectations with respect to the target distribution, which can be generated in parallel and averaged, as well as estimates of the finite-time bias of the underlying MCMC algorithm. Crucially, this information is retrieved from the distribution of the meeting time, which is an integer-valued random variable irrespective of the dimension of the problem, and thus provides a convenient summary of the performance of the algorithm. A difficulty inherent to the approach is the design of an effective coupling strategy, which must be done on a per-algorithm basis. High-dimensional parameter spaces add a substantial layer of complication as standard strategies based on maximal couplings may be inadequate.

1.3 Our contribution

We develop couplings of Gibbs samplers for Bayesian linear regression with Half- $t(\nu)$ local shrinkage priors, and make several contributions.

We introduce blocked Gibbs samplers (Section 2) for Bayesian linear regression with Half- $t(\nu)$ local shrinkage priors, extending the algorithm of Johndrow et al. [2020] for the Horseshoe. Our algorithm has an overall computation cost of $\mathcal{O}(n^2p)$ per iteration, which is state-of-the-art for $n \ll p$. We show that a variant of this Gibbs sampler satisfies a geometric drift condition (Proposition 2.3) and a minorization condition (Proposition 2.4), and thus that it is geometrically ergodic. These results can in turn allow to check that the meeting times have exponential tails. Despite a decade of widespread use, MCMC algorithms for the Horseshoe and Half- $t(\nu)$ priors generally have not previously been shown to be geometrically ergodic, contrarily to MCMC algorithms for global-local models with exponentially-tailed local scale priors [Khare and Hobert, 2013, Pal and Khare, 2014]. Our proofs utilize a uniform bound on generalized ridge regression estimates, which enables us to avoid a technical assumption of Johndrow et al. [2020], and auxiliary results on moments of distributions related to the confluent hypergeometric function of the second kind. Shortly after an earlier version of this manuscript was posted, Bhattacharya et al. [2021] have also established geometric ergodicity of other related Gibbs samplers for the Horseshoe prior.

We design coupling strategies for these Gibbs samplers (Section 3). We develop a *two-scale* strategy, based on a carefully chosen metric, which informs the choice between synchronous and maximal couplings. This strategy leads to orders of magnitude shorter meeting times compared to the naïve approach, as illustrated in Figure 1a. For our two-scale coupling, we further highlight that priors with stronger shrinkage towards zero can give significantly shorter meeting times in high dimensions. This motivates usage of Half- $t(\nu)$ priors with greater degrees of freedom $\nu > 1$, which can give similar statistical performance to the Horseshoe ($\nu = 1$) whilst enjoying orders of magnitude computational improvements. Figures 1b and 1c highlight this trade-off between computation and statistical estimation.

Finally, we demonstrate (Section 4) that the proposed coupled MCMC algorithm is applicable to big data settings. Figure 1d highlights an application of our coupling strategy to monitor the convergence of the Gibbs sampler for Bayesian regression on a genome-wide association study (GWAS) dataset with $(n, p) \approx (2000, 100000)$. Our method suggests that a burn-in of just 700 iterations can suffice even for such a large problem, and confirms the applicability of coupled MCMC algorithms for practical high-dimensional inference.

Anonymized scripts in R [R Core Team, 2013] are available from <https://github.com/niloyb/CoupledHalfT> to reproduce the figures of the article.

2 MCMC for regression with Half- $t(\nu)$ priors

We develop an MCMC algorithm for Bayesian shrinkage regression with Half- $t(\nu)$ priors. The model is given by (1)–(2) and $\eta^{-1/2} \sim t(\nu)$ for some $\nu \geq 1$ as in (3). In Section 2.1, we first derive the marginal posterior distribution of β and discuss challenges in constructing MCMC algorithms for these targets. In Section 2.2, we introduce Gibbs samplers for such targets and establish geometric ergodicity of a variant of our samplers. This result, in conjunction with a result in Jacob et al. [2020, Proposition 3.4], allows us to check that the meeting times have exponential tails, which in turn justifies the application of couplings for bounding mixing times and obtaining unbiased estimates in the remainder of the paper.

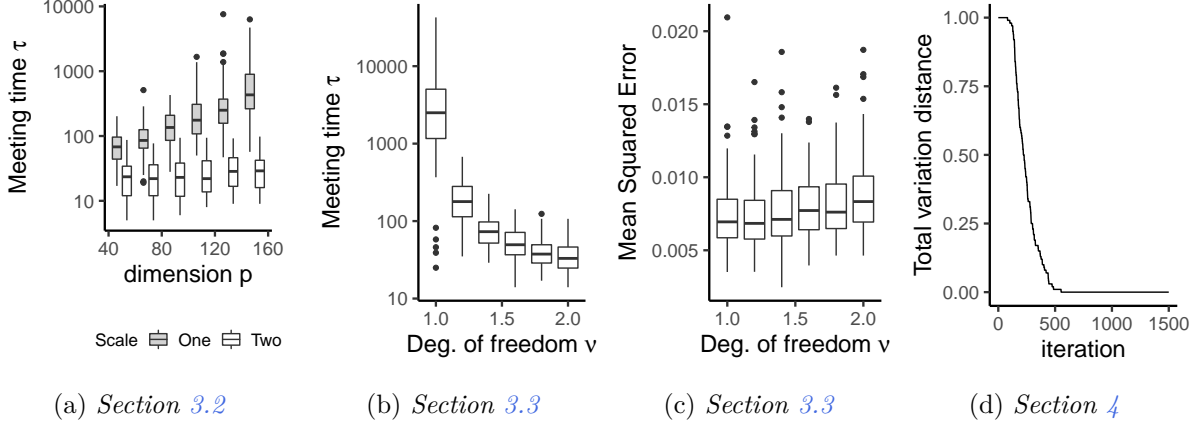


Figure 1: Highlights of our contribution. Figures 1a and 1b plot meeting times τ , Figure 1c plots the mean squared error under Half- $t(\nu)$ priors, and Figure 1d plots upper bounds on the total variation between the chain and the target distribution against iteration.

2.1 Features of the target complicate use of generic MCMC

While posterior distributions resulting from heavy-tailed shrinkage priors have desirable statistical properties, their features pose challenges to generic MCMC algorithms. For Half- $t(\nu)$ priors, we show that the resulting posterior distributions present 1) multimodality, 2) heavy tails and 3) poles at zero. This hints at a trade-off between statistical accuracy and computational difficulty, since the very features that present computational challenges are crucial for optimal statistical performance across sparsity levels and signal strengths.

Proposition 2.1 gives the marginal prior and posterior densities of (β, σ^2, ξ) up to normalizing constants, i.e. integrating over η . For any real-valued functions f and g , we write $f(x) \asymp g(x)$ for $x \rightarrow x_0$ when $m < \liminf_{x \rightarrow x_0} |f(x)/g(x)| \leq \limsup_{x \rightarrow x_0} |f(x)/g(x)| < M$ for some $0 < m \leq M < \infty$.

Proposition 2.1. *The marginal prior of component β_j on \mathbb{R} given ξ and σ^2 has density*

$$\pi(\beta_j | \xi, \sigma^2) \propto U\left(\frac{1+\nu}{2}, 1, \frac{\xi \beta_j^2}{2\sigma^2 \nu}\right) \asymp \begin{cases} -\log |\beta_j| & \text{for } |\beta_j| \rightarrow 0 \\ |\beta_j|^{-(1+\nu)} & \text{for } |\beta_j| \rightarrow +\infty \end{cases}, \quad (4)$$

where $\Gamma(\cdot)$ is the Gamma function, and $U(a, b, z) := \Gamma(a)^{-1} \int_0^\infty x^{a-1} (1+x)^{b-a-1} e^{-zx} dx$ is the confluent hypergeometric function of the second kind [Abramowitz, 1974, Section 13] for any $a, b, z > 0$. The marginal posterior density of β on \mathbb{R}^p given ξ and σ^2 is

$$\pi(\beta | \sigma^2, \xi, y) \propto \mathcal{N}(y; X\beta, \sigma^2 I_n) \prod_{j=1}^p U\left(\frac{1+\nu}{2}, 1, \frac{\xi \beta_j^2}{2\sigma^2 \nu}\right), \quad (5)$$

thus $\pi(\beta | \sigma^2, \xi, y) \stackrel{\|\beta\| \rightarrow 0}{\asymp} -\prod_{j=1}^p \log(|\beta_j|)$ and $-\frac{\partial}{\partial \beta_j} \log \pi(\beta | \sigma^2, \xi, y) \stackrel{\beta_j \rightarrow 0}{\asymp} -(\beta_j \log |\beta_j|)^{-1}$.

Figure 2 gives an example of such marginal posterior in a stylized setting. Here

$$n = 2, \quad p = 3, \quad X = \begin{pmatrix} 1 & 1 & 0 \\ 1 & 0 & 1 \end{pmatrix}, \quad y = X(1 \ 0 \ 0)^T = (1 \ 1)^T,$$

with $\nu = 2$ and $\xi = \sigma^2 = 0.25$. Component β_1 in Figure 2 illustrates the potential multimodality in the posterior. The posterior distribution also has polynomial tails in high dimensions, as stated in Corollary 2.2.

Corollary 2.2. *Let $\beta^\perp \in \mathbb{R}^p$ be any unit vector such that $X\beta^\perp = 0$ and let $\lambda > 0$. Then*

$$\pi(\lambda \beta^\perp | \sigma^2, \xi, y) \asymp \lambda^{-p(1+\nu)}$$

for $\lambda \rightarrow +\infty$. That is, the marginal posterior of β on \mathbb{R}^p has polynomial tails along all directions in the null space $\ker(X)$ of X .

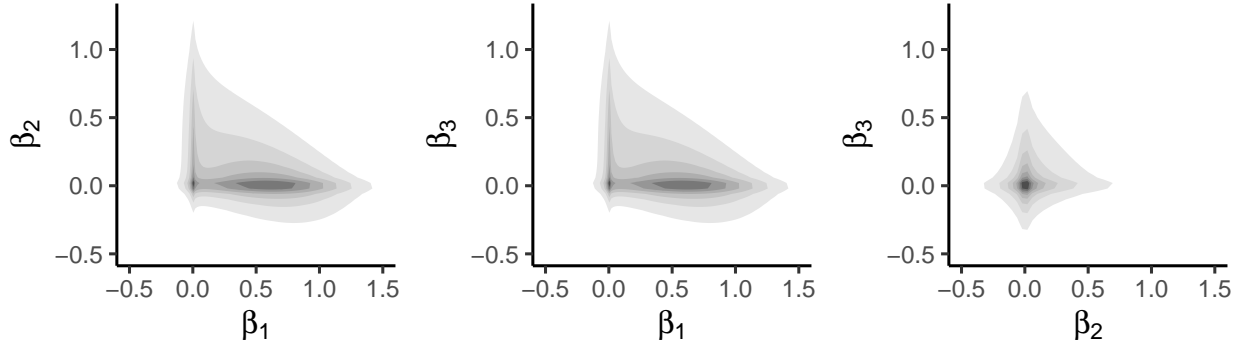


Figure 2: Posterior densities $\pi(\beta_1, \beta_2 | \sigma^2, \xi, y)$, $\pi(\beta_1, \beta_3 | \sigma^2, \xi, y)$ and $\pi(\beta_2, \beta_3 | \sigma^2, \xi, y)$.

In our stylized example, $\beta^\perp = 3^{-1/2}(1 - 1 - 1)^T$ satisfies $X\beta^\perp = 0$. It follows from Corollary 2.2 that $\pi(\lambda\beta^\perp | \sigma^2, \xi, y) \asymp \lambda^{-3(1+\nu)} \asymp \lambda^{-9}$ for large λ . More generally, whenever $p > n$ and the marginal prior on β has polynomial tails, the subspace $\ker(X)$ of \mathbb{R}^p has vector space dimension at least $(p - n)$, and therefore the posterior has polynomial tails over a non-trivial subspace. For such heavy-tailed targets, the most popular “generic” MCMC algorithms encounter significant theoretical and practical challenges. Here, we use the term generic for algorithms that are not explicitly designed to target this class of distributions, but instead rely on a general strategy to explore state spaces. Specifically, for heavy-tailed targets, *lack* of geometric ergodicity has been established for Random Walk Metropolis–Hastings (RWMH) [Jarner and Tweedie, 2003], Metropolis-Adjusted Langevin (MALA) [Roberts and Tweedie, 1996] and Hamiltonian Monte Carlo (HMC) [Livingstone et al., 2019a]¹. Better performance can sometimes be obtained using heavy-tailed proposals [Jarner and Roberts, 2007, Sherlock et al., 2010, Livingstone et al., 2019b] or variable transformations when available [Johnson and Geyer, 2012].

The posterior density in Equation (5) also approaches infinity when any component β_j approaches zero, as $\lim_{\beta_j \rightarrow 0} U((1+\nu)/2, 1, (\xi\beta_j^2)/(2\sigma^2\nu)) = \infty$ for any $\nu, \xi, \sigma^2 > 0$. This is highlighted by the modes at the origin in Figure 2. The *pole* at zero corresponds to a discontinuity in the gradients of the negative log-density, as given in Proposition 2.1. Such diverging gradients can lead to numerically unstable leapfrog integration for HMC samplers [Bou-Rabee and Sanz-Serna, 2018].

With these challenges in mind we next describe a Gibbs sampler tailored for the class of target under consideration. We will show that it is geometrically ergodic without any additional assumptions on the design matrix X or the values of n and p , and we will use a coupling approach and extensive numerical experiments to assess its practical performance.

2.2 A blocked Gibbs sampler for Half- $t(\nu)$ priors

Blocked Gibbs samplers are popularly used for Bayesian regression with global-local shrinkage priors, due to the analytical tractability of full-conditional distributions, which exploits the conditional Gaussian representation of the prior; see Park and Casella [2008], Carvalho et al. [2010], Polson et al. [2014], Bhattacharya et al. [2015], Makalic and Schmidt [2016] for some representative examples. Several convenient blocking and marginalization strategies are possible, leading to conditionals that are easy to sample from. For the case of the Horseshoe prior ($\nu = 1$), Johndrow et al. [2020] have recently developed exact and approximate MCMC algorithms which are scalable to high-dimensional settings. Their approach is based on a blocked Gibbs sampler, building on earlier algorithms of Polson et al. [2014] and Bhattacharya et al. [2016]. We extend the blocked Gibbs sampler of Johndrow et al. [2020] for the Horseshoe to general Half- $t(\nu)$ priors. The proposed Gibbs sampler is described in Algorithm 1 below. Derivations are deferred to Appendix D.

¹Jarner and Tweedie [2003], Roberts and Tweedie [1996] and Livingstone et al. [2019a] show lack of geometric ergodicity for targets which have heavy-tails in every direction. Their arguments can be modified to hold for targets which are heavy-tailed along any one direction as in Corollary 2.2, by considering a projection of the full chain along that direction.

Algorithm 1: MCMC for Bayesian shrinkage regression with Half- $t(\nu)$ priors.

Input: $C_t := (\beta_t, \eta_t, \sigma_t^2, \xi_t) \in \mathbb{R}^p \times \mathbb{R}_{>0}^p \times \mathbb{R}_{>0} \times \mathbb{R}_{>0}$.

1. Sample $\eta_{t+1} | \beta_t, \sigma_t^2, \xi_t$ component-wise independently using Algorithm 2, targeting

$$\pi(\eta_{t+1} | \beta_t, \sigma_t^2, \xi_t) \propto \prod_{j=1}^p \pi(\eta_{j,t+1} | m_{j,t} := \frac{\xi_t \beta_{j,t}^2}{2\sigma_t^2}) \propto \prod_{j=1}^p \frac{e^{-m_{j,t} \eta_{j,t+1}}}{\eta_{j,t+1}^{\frac{1-\nu}{2}} (1 + \nu \eta_{j,t+1})^{\frac{\nu+1}{2}}}.$$

2. Sample $\xi_{t+1}, \sigma_{t+1}^2, \beta_{t+1}$ given η_{t+1} as follows:

- (a) Sample ξ_{t+1} using Metropolis–Hastings with step-size σ_{MH} :

Given ξ_t , propose $\log(\xi^*) \sim \mathcal{N}(\log(\xi_t), \sigma_{\text{MH}}^2)$.

Calculate acceptance probability

$$q = \frac{L(y|\xi_*, \eta_{t+1})\pi_\xi(\xi_*)}{L(y|\xi_t, \eta_{t+1})\pi_\xi(\xi_t)} \frac{\xi^*}{\xi_t},$$

where $\pi_\xi(\cdot)$ is the prior for ξ , $M_{\xi,\eta} := I_n + \xi^{-1} X Diag(\eta^{-1}) X^T$ and

$$\log(L(y|\xi, \eta)) = -\frac{1}{2} \log(|M_{\xi,\eta}|) - \frac{a_0 + n}{2} \log(b_0 + y^T M_{\xi,\eta}^{-1} y). \quad (6)$$

Set $\xi_{t+1} := \xi^*$ with probability $\min(1, q)$, otherwise set $\xi_{t+1} := \xi_t$.

- (b) Sample σ_{t+1}^2 given ξ_{t+1}, η_{t+1} :

$$\sigma_{t+1}^2 | \xi_{t+1}, \eta_{t+1} \sim \text{InvGamma}\left(\frac{a_0 + n}{2}, \frac{y^T M_{\xi_{t+1}, \eta_{t+1}}^{-1} y + b_0}{2}\right).$$

- (c) Sample β_{t+1} given $\sigma_{t+1}^2, \xi_{t+1}, \eta_{t+1}$ using Algorithm 9 in Appendix C, targeting

$$\beta_{t+1} | \sigma_{t+1}^2, \xi_{t+1}, \eta_{t+1} \sim \mathcal{N}(\Sigma^{-1} X^T y, \sigma_{t+1}^2 \Sigma^{-1}) \text{ for } \Sigma = X^T X + \xi_{t+1} Diag(\eta_{t+1}).$$

return $C_{t+1} := (\beta_{t+1}, \eta_{t+1}, \sigma_{t+1}^2, \xi_{t+1})$.

Algorithm 2: Slice Sampling for Half- $t(\nu)$ prior.

Result: Slice sampler targeting $p(\eta_j|m_j) \propto (\eta_j^{\frac{1-\nu}{2}} (1 + \nu\eta_j)^{\frac{\nu+1}{2}})^{-1} e^{-m_j\eta_j}$ on $(0, \infty)$.

Input: $m_j > 0$, state $\eta_{j,t} > 0$.

1. Sample $U_{j,t}|\eta_{j,t} \sim \text{Uniform}(0, (1 + \nu\eta_{j,t})^{-\frac{\nu+1}{2}})$.

2. Sample $\eta_{j,t+1}|U_{j,t} \sim P_j$, where distribution P_j has unnormalized density $\eta_{j,t+1}^{s-1} e^{-m_j\eta_{j,t+1}}$ on $(0, T_{j,t})$ for $T_{j,t} = (U_{j,t}^{-\frac{2}{1+\nu}} - 1)/\nu$ and $s = \frac{1+\nu}{2}$. Sample $\eta_{j,t+1}$ perfectly such that

$$\eta_{j,t+1} = \frac{1}{m_j} \gamma_s^{-1} \left(\gamma_s(m_j T_{j,t}) U^* \right) \text{ for } U^* \sim \text{Uniform}(0, 1),$$

where $\gamma_s(x) := \frac{1}{\Gamma(s)} \int_0^x t^{s-1} e^{-t} dt \in [0, 1]$ is the cumulative distribution function of a $\text{Gamma}(s, 1)$ distribution.

return $\eta_{j,t+1}$.

Computation Cost. Step (1) of Algorithm 1 (component-wise slice sampling) is an $\mathcal{O}(p)$ cost operation. Step 2(a) involves an $\mathcal{O}(n^2p)$ cost operation (calculating the weighted matrix cross-product $X \text{Diag}(\eta)^{-1} X^T$) and an $\mathcal{O}(n^3)$ cost operation (calculating $y^T M_{\xi,\eta}^{-1} y$ and $|M_{\xi,\eta}|$ in Equation (6) using Cholesky decomposition). Step 2(b) is only an $\mathcal{O}(1)$ cost operation, as $y^T M_{\xi,\eta}^{-1} y$ is pre-calculated in Step 2(a). Similarly, as $M_{\xi,\eta}^{-1}$ is pre-calculated in Step 2(a), Step 2(c) only involves an $\mathcal{O}(np)$ and an $\mathcal{O}(n^2)$ cost operation (calculating terms Xu and $M_{\xi,\eta}^{-1}(\frac{y}{\sigma} - v)$ in Algorithm 9 respectively). In high-dimensional settings with $p > n$, which is our focus, the weighted matrix cross-product calculation is the most expensive and overall Algorithm 1 has $\mathcal{O}(n^2p)$ computation cost.

Geometric Ergodicity. We establish geometric ergodicity for the blocked Gibbs sampler in Algorithm 1. For a class of Gibbs samplers targeting shrinkage priors including the Bayesian LASSO, the Normal-Gamma prior [Griffin and Brown, 2010], and Dirichlet-Laplace prior [Bhattacharya et al., 2015], Khare and Hobert [2013] and Pal and Khare [2014] have proven geometric ergodicity based on drift and minorization arguments [Meyn and Tweedie, 1993, Roberts and Rosenthal, 2004]. For the Horseshoe prior, Johndrow et al. [2020] has recently established geometric ergodicity. In the high-dimensional setting with $p > n$ for the Horseshoe, the proof of Johndrow et al. [2020] required a truncation of the prior on each η_j to exclude the origin. Here we prove geometric ergodicity for Half- $t(\nu)$ priors including the Horseshoe ($\nu = 1$) in both low and high-dimensional settings, without any modification of the priors on the η_j .

We assume that the global shrinkage prior $\pi_\xi(\cdot)$ has a compact support on $(0, \infty)$. Such compactly supported priors or an empirical Bayes estimator for ξ have been recommended by van der Pas et al. [2017] to achieve near optimal posterior concentration for the Horseshoe in the Normal means model. For simplicity, our analysis assumes that we sample $\xi|\eta$ (Step (2)(a) of Algorithm 1) perfectly instead of using Metropolis-Hastings, and that we sample each $\eta_j|\beta_j, \xi, \sigma^2$ component-wise (Step (1) of Algorithm 1) perfectly instead of using a slice sampler. Then the blocked Gibbs sampler of Algorithm 1 can be re-expressed as:

$$\begin{aligned} \pi(\eta_{t+1}|\beta_t, \sigma_t^2, \xi_t) &\propto \prod_{j=1}^p \frac{e^{-m_{j,t}\eta_{j,t+1}}}{\eta_{j,t+1}^{\frac{1-\nu}{2}} (1 + \nu\eta_{j,t+1})^{\frac{\nu+1}{2}}} \text{ for } m_{j,t} = \frac{\xi_t \beta_{j,t}^2}{2\sigma_t^2}, \\ \pi(\xi_{t+1}|\eta_{t+1}) &\propto L(y|\xi_{t+1}, \eta_{t+1})\pi_\xi(\xi_{t+1}), \\ \sigma_{t+1}^2|\eta_{t+1}, \xi_{t+1} &\sim \text{InvGamma}\left(\frac{a_0 + n}{2}, \frac{y^T M_{\xi_{t+1}, \eta_{t+1}}^{-1} y + b_0}{2}\right), \\ \beta_{t+1}|\eta_{t+1}, \xi_{t+1}, \sigma_{t+1}^2 &\sim \mathcal{N}(\Sigma^{-1} X^T y, \sigma_{t+1}^2 \Sigma^{-1}). \end{aligned} \tag{7}$$

Perfect sampling algorithms for $\xi|\eta$ and $\eta_j|\beta_j, \xi, \sigma^2$ component-wise are provided in Algorithms 12 and 13 of Appendix C for completeness. Compared to Algorithm 1, perfectly sampling $\xi|\eta$ and $\eta_j|\beta_j, \xi, \sigma^2$ also

gives $\mathcal{O}(n^2 p)$ computational cost for the full blocked Gibbs sampler, but in practice this implementation is more expensive per iteration due to the computation of eigenvalue decompositions in lieu of Cholesky decompositions, and the computation of inverse of the confluent hypergeometric function of the second kind.

Our main results about the Gibbs sampler are given in Propositions 2.3 and 2.4.

Proposition 2.3. *(Geometric drift). Consider the Markov chain $(\beta_t, \xi_t, \sigma_t^2)_{t \geq 0}$ generated from the blocked Gibbs sampler in Equation (7), such that $(\beta_t, \xi_t, \sigma_t^2) \mapsto \eta_{t+1} \mapsto (\beta_{t+1}, \xi_{t+1}, \sigma_{t+1}^2)$ with η_{t+1} intermediary for each $t \geq 0$. Assume the global shrinkage prior $\pi_\xi(\cdot)$ has a compact support. For $m_j = \xi \beta_j^2 / (2\sigma^2)$, $c \in (0, 1/2)$ and $d \in (0, 1)$, define*

$$V(\beta, \xi, \sigma^2) = \sum_{j=1}^p m_j^{-c} + m_j^d. \quad (8)$$

Then for each $\nu \geq 1$, there exist some $c \in (0, 1/2)$, $d \in (0, 1)$ such that V is a Lyapunov function. That is, there exists some $\gamma \in (0, 1)$ and $K \in (0, \infty)$ such that

$$\mathbb{E}[V(\beta_{t+1}, \xi_{t+1}, \sigma_{t+1}^2) | \beta_t, \xi_t, \sigma_t^2] \leq \gamma V(\beta_t, \xi_t, \sigma_t^2) + K \quad \text{for all } \beta_t \in \mathbb{R}^p, \xi_t > 0 \text{ and } \sigma_t^2 > 0.$$

The Lyapunov function in (8), approaches infinity when any β_j approaches the origin or infinity. This ensures that the sub-level sets (as defined in Proposition 2.4) exclude the pole at the origin and are bounded. A key insight in our proof is the application of a uniform bound on generalized ridge regression estimates (Lemma A.1 in Appendix A),

$$\sup_{\eta \in (0, \infty)^p} \|(X^T X + \xi \text{Diag}(\eta))^{-1} X^T y\|_2 = \|X^\dagger y\|_2, \quad (9)$$

for $\|\cdot\|_2$ the L_2 norm and X^\dagger the Moore-Penrose pseudoinverse of matrix X . When $n \geq p$, $X^\dagger = (X^T X)^{-1} X^T$ and we recover the well-known result [Hoerl and Kennard, 1970] that ridge regression produces estimates with smaller norms compared to ordinary least squares. Equation (9) generalizes this insight to the high-dimensional setting. In comparison, Johndrow et al. [2020] considered the bound $\|(X^T X + \xi \text{Diag}(\eta))^{-1} X^T y\|_2 \leq \|(\xi \text{Diag}(\eta))^{-1} X^T y\|_2$ for the Horseshoe prior. This required truncating the prior on each η_j below by a small $\ell > 0$ to guarantee the uniform bound $\eta_j \geq \ell$.

Proposition 2.4. *(Minorization condition). For $R > 0$, let $S(R) = \{(\beta, \xi, \sigma^2) \in \mathbb{R}^p \times \mathbb{R}_{>0} \times \mathbb{R}_{>0} : V(\beta, \xi, \sigma) < R\}$ denote the sub-level sets of the Lyapunov function in Proposition 2.3. Let \mathcal{P} denote the Markov transition kernel associated with the update from $(\beta_t, \xi_t, \sigma_t^2)$ to $(\beta_{t+1}, \xi_{t+1}, \sigma_{t+1}^2)$ implied by the update rule in (7). Let $Z^{(i)} = (\beta^{(i)}, \xi^{(i)}, (\sigma^{(i)})^2)$ for $i = 1, 2$. Then for all $R > 0$, there exists $\epsilon \in (0, 1)$ such that*

$$d_{TV}(\mathcal{P}(Z^{(1)}, \cdot), \mathcal{P}(Z^{(2)}, \cdot)) < 1 - \epsilon \quad \text{for all } Z^{(1)}, Z^{(2)} \in S(R).$$

In particular for $R > 1$, $\epsilon = (U(\frac{1+\nu}{2}, 1, \frac{R^{1/d}}{\nu}) / U(\frac{1+\nu}{2}, 1, \frac{R^{-1/c}}{\nu}))^p$ suffices.

Geometric ergodicity now directly follows from Proposition 2.3 and Proposition 2.4 with any $R > \max\{1, 2K/(1 - \gamma)\}$ (see Rosenthal [1995]). From the proof of Proposition 2.4, note that ϵ approaches zero exponentially as a function of dimension p . This is consistent with the observation that drift and “one step” minorization based total variation bounds often yield contraction rates which approach 1 exponentially fast with increasing dimension [Rajaratnam and Sparks, 2015, Qin and Hobert, 2019, 2020]. The behavior of the algorithm in increasing dimensions is investigated empirically using the couplings introduced in Section 3. The use of these couplings to obtain a more precise convergence analysis is an interesting avenue of future work, discussed in Section 5.

Remark 2.5. *Our proofs generalize to a larger class of priors satisfying some moment conditions on the full conditionals of η_j . Consider a compactly supported prior π_ξ on ξ , and a prior π_η on each η_j . Then the unnormalized density of the full conditionals of each η_j is given by*

$$\pi(\eta_j | m_j = \xi \beta_j^2 / (2\sigma^2)) \propto \eta_j^{1/2} \exp(-m_j \eta_j) \pi_\eta(\eta_j).$$

Consider the following assumptions on π_η .

1. For some $0 < c < 1/2$, there exist $0 < \epsilon < \Gamma(\frac{1}{2} - c)^{-1} \sqrt{\pi}$ and $K_{c,\epsilon}^{(1)} < \infty$ such that

$$\mathbb{E}[\eta_j^c | m_j] \leq \epsilon m_j^{-c} + K_{c,\epsilon}^{(1)} \quad \text{for all } m_j > 0.$$

2. For some $0 < d < 1$, there exist $0 < \epsilon < 2^d$ and $K_{d,\epsilon}^{(2)} < \infty$ such that

$$\mathbb{E}[\eta_j^{-d} | m_j] \leq \epsilon m_j^d + K_{d,\epsilon}^{(2)} \quad \text{for all } m_j > 0.$$

Then the blocked Gibbs sampler in (7) is geometrically ergodic.

3 Coupling strategies for the proposed Gibbs sampler

We develop couplings for the blocked Gibbs sampler presented in Section 2. We will be particularly interested in coupled chains generated with a time lag $L \geq 1$ in order to implement the diagnostics of convergence proposed in Biswas et al. [2019]. Consider an L -lag coupled chain $(C_t^{(1)}, C_{t-L}^{(2)})_{t \geq L}$ with meeting time $\tau := \inf\{t \geq L : C_t^{(1)} = C_{t-L}^{(2)}\}$. Recall that each C_t stands for the full state $(\beta_t, \eta_t, \sigma_t^2, \xi_t)$ as defined in Algorithm 1. For the coupling-based methods proposed in Biswas et al. [2019], Jacob et al. [2020] to be most practical, we want the meeting times to occur as early as possible, under the constraint that both $(C_t^{(i)})_{t \geq 0}$, $i = 1, 2$ start from the same initial distribution, here taken to be the prior distribution, and that they both evolve according to the blocked Gibbs sampler.

In Section 3.1, we consider a maximal coupling-based algorithm and highlight difficulties in scaling such an algorithm in high dimensions. In Section 3.2, we carefully develop a *two-scale* coupling that delivers better performance. In Section 3.3, we investigate the impact of the degree of freedom ν for Half- $t(\nu)$ priors on our two-scale coupling. We find that Half- $t(\nu)$ priors with higher degrees of freedom $\nu > 1$ can give similar statistical performance to the Horseshoe ($\nu = 1$), whilst enjoying orders of magnitude computational improvements through shorter coupling times. For simplicity, we mostly omit the lag L from the notation.

3.1 A one-scale coupling

For the blocked Gibbs sampler in Algorithm 1, we first consider a coupled MCMC algorithm that attempts exact meetings at every step. We will apply a maximal coupling algorithm with independent residuals (see Thorisson [2000, Chapter 1 Section 4.4] and Johnson [1998]). It is included in Algorithm 7 of Appendix C, and has an expected computation cost of two units [Jacob et al., 2020].

Our initial coupled MCMC kernel is given in Algorithm 3, which we refer to as a *one-scale* coupling. That is, before the chains have met (when $C_t^{(1)} \neq C_t^{(2)}$), the coupled kernel on Steps (1) and (2)(a–c) does not explicitly depend on the distance between states $C_t^{(1)}$ and $C_t^{(2)}$. After meeting, the coupled chains remain together by construction, such that $C_t^{(1)} = C_t^{(2)}$ implies $C_{t+1}^{(1)} = C_{t+1}^{(2)}$. When $C_t^{(1)} \neq C_t^{(2)}$, Step (1) uses the coupled slice sampler of Algorithm 4 component-wise for $(\eta_{t+1}^{(1)}, \eta_{t+1}^{(2)})$, which allows each pair of components $(\eta_{j,t+1}^{(1)}, \eta_{j,t+1}^{(2)})$ to meet exactly with positive probability. In Algorithm 4, we use a common random numbers or a ‘synchronous’ coupling of the auxiliary random variables $(U_{j,*}^{(1)}, U_{j,*}^{(2)})$, and alternative couplings could be considered. Steps (2)(a–b) are maximal couplings of the conditional sampling steps for $(\xi^{(1)}, \xi^{(2)})$ and $(\sigma^{(1)}, \sigma^{(2)})$, such that $(\sigma_{t+1}^{(1)}, \xi_{t+1}^{(1)}, \eta_{t+1}^{(1)}) = (\sigma_{t+1}^{(2)}, \xi_{t+1}^{(2)}, \eta_{t+1}^{(2)})$ occurs with positive probability for all $t \geq 0$. Step (2)(c) uses common random numbers coupling, such that $(\sigma_{t+1}^{(1)}, \xi_{t+1}^{(1)}, \eta_{t+1}^{(1)}) = (\sigma_{t+1}^{(2)}, \xi_{t+1}^{(2)}, \eta_{t+1}^{(2)})$ implies $\beta_{t+1}^{(1)} = \beta_{t+1}^{(2)}$. This allows the full chains to meet exactly with positive probability at every step.

Simulations. We consider the performance of Algorithm 3 on synthetic datasets. For number of observations n and dimension p , the synthetic dataset (X, y) is generated by a design matrix $X \in \mathbb{R}^{n \times p}$ with $[X]_{i,j} \stackrel{i.i.d.}{\sim} \mathcal{N}(0, 1)$ and a response vector $y \sim \mathcal{N}(X\beta_*, \sigma_*^2 I_n)$, where $\beta_* \in \mathbb{R}^p$ is the true signal and $\sigma_* \geq 0$ is the true error standard deviation. We choose β_* to be sparse such that for sparsity parameter s , $\beta_{*,j} = 2^{(9-j)/4}$ for $1 \leq j \leq s$ and $\beta_{*,j} = 0$ for all $s > j$. Figure 3 shows the meeting times τ of coupled Markov chains

Algorithm 3: A one-scale coupled MCMC kernel for Half- $t(\nu)$ priors.

Input: $C_t^{(i)} := (\beta_t^{(i)}, \eta_t^{(i)}, (\sigma_t^{(i)})^2, \xi_t^{(i)}) \in \mathbb{R}^p \times \mathbb{R}_{>0}^p \times \mathbb{R}_{>0} \times \mathbb{R}_{>0}$ for chains $i = 1, 2$.

if $C_t^{(1)} = C_t^{(2)}$ **then** Sample $C_{t+1}^{(1)}|C_t^{(1)}$ using Algorithm 1 and set $C_{t+1}^{(2)} = C_{t+1}^{(1)}$.

else

1. Sample $(\eta_{t+1}^{(1)}, \eta_{t+1}^{(2)})|C_t^{(1)}, C_t^{(2)}$ component-wise independently using Algorithm 4.
2. Sample $((\xi_{t+1}^{(1)}, (\sigma_{t+1}^{(1)})^2, \beta_{t+1}^{(1)}), (\xi_{t+1}^{(2)}, (\sigma_{t+1}^{(2)})^2, \beta_{t+1}^{(2)})$ given $\eta_{t+1}^{(1)}, \eta_{t+1}^{(2)}$ as follows:
 - (a) Sample $(\xi_{t+1}^{(1)}, \xi_{t+1}^{(2)})|\eta_{t+1}^{(1)}, \eta_{t+1}^{(2)}, \xi_t^{(1)}, \xi_t^{(2)}$ using coupled Metropolis–Hastings (Algorithm 11 in Appendix C).
 - (b) Sample $((\sigma_{t+1}^{(1)})^2, (\sigma_{t+1}^{(2)})^2)|\xi_{t+1}^{(1)}, \eta_{t+1}^{(1)}, \xi_{t+1}^{(2)}, \eta_{t+1}^{(2)}$ from a maximal coupling of two Inverse Gamma distributions (Algorithm 7 in Appendix C).
 - (c) Sample $(\beta_{t+1}^{(1)}, \beta_{t+1}^{(2)})|(\sigma_{t+1}^{(1)})^2, \xi_{t+1}^{(1)}, \eta_{t+1}^{(1)}, (\sigma_{t+1}^{(2)})^2, \xi_{t+1}^{(2)}, \eta_{t+1}^{(2)}$ using a common random numbers coupling of Normals for Gaussian scale mixture priors (Algorithm 10 in Appendix C).

return $(C_{t+1}^{(1)}, C_{t+1}^{(2)})$.

Algorithm 4: Coupled Slice Sampler for Half- $t(\nu)$ priors using maximal couplings.

Input: $\eta_{j,t}^{(1)}, \eta_{j,t}^{(2)}, m_{j,t}^{(1)} := \frac{\xi_t^{(1)}(\beta_{j,t}^{(1)})^2}{2(\sigma_t^{(1)})^2}, m_{j,t}^{(2)} := \frac{\xi_t^{(2)}(\beta_{j,t}^{(2)})^2}{2(\sigma_t^{(2)})^2} > 0$.

1. Sample $U_{j,*}^{crn} \sim \text{Uniform}(0, 1)$, and set $U_{j,*}^{(1)} := U_{j,*}^{crn}(1 + \nu\eta_{j,t}^{(i)})^{-\frac{\nu+1}{2}}$ for $i = 1, 2$.
2. Sample $(\eta_{j,t+1}^{(1)}, \eta_{j,t+1}^{(2)})|U_{j,*}^{(1)}, U_{j,*}^{(2)}$ from a maximal coupling of $P_j^{(1)}$ and $P_j^{(2)}$ using Algorithm 7 in Appendix C, where each marginal distribution $P_j^{(i)}$ corresponds to distribution P_j of the slice sampler of Algorithm 2.

return $(\eta_{j,t+1}^{(1)}, \eta_{j,t+1}^{(2)})$.

(with a lag $L = 1$) targeting the Horseshoe posterior ($\nu = 1$) with $a_0 = b_0 = 1$ under Algorithm 3. We initialize both chains independently at the prior distribution (Equation (2)). For the ξ updates, we use a Metropolis–Hastings step-size of $\sigma_{\text{MH}} = 0.8$ as in [Johnstone et al., 2020]. Each sub-figure plots kernel density estimates of τ against each parameter n, p, s, σ_* respectively, based on 100 independent replicate simulations. Figure 3a shows that the meeting times tend to decrease with more observations. Figures 3b, 3c and 3d show that the meeting times tend to increase exponentially and have heavier tails with increasing dimensions, sparsity parameter and the true error standard deviation respectively.

3.2 A two-scale coupling

To address the scaling issues observed with the one-scale coupling, we develop a *two-scale* coupling. This refers to coupled kernels that attempt exact meetings when the chains are close, and aim for a contraction when the chains are far. This differs from the terminology used in stochastic dynamics and in analysis of pre-conditioned HMC [Bou-Rabee and Eberle, 2020]. The motivation for this construction is that in Algorithm 3, the components of $(\eta_t^{(1)}, \eta_t^{(2)})$ that fail to meet instead evolve independently. As dimension grows, the number of components of $(\eta_t^{(1)}, \eta_t^{(2)})$ that fail to meet also tends to grow, making it increasingly difficult for all components to exactly meet on subsequent iterations. We therefore only attempt exact meetings when the associated meeting probability is high enough. This is done by constructing a metric d such that when the current states are d -close, the probability that *all* of the components of $(\eta_t^{(1)}, \eta_t^{(2)})$ meet is high.

Our two-scale coupling for a generic metric d and corresponding threshold parameter $d_{\text{threshold}} \geq 0$ is

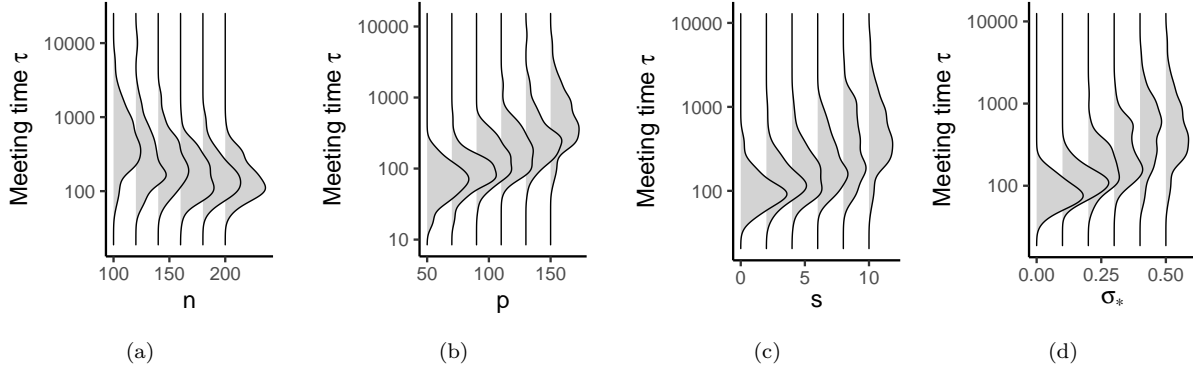


Figure 3: Meeting times for posteriors associated with a Horseshoe prior under the one-scale coupling of Algorithm 3. Unless specified otherwise, $n = 100, p = 150, s = 10, \sigma_* = 0.5$.

given in Algorithm 5. When the chains are *close* with $d(C_t^{(1)}, C_t^{(2)}) \leq d_{threshold}$, we apply Algorithm 4 and attempt to exactly meet. When the chains are *far away* with $d(C_t^{(1)}, C_t^{(2)}) > d_{threshold}$, we instead apply the common random numbers coupling of Algorithm 6. As we observe empirically, common random numbers coupling results in contraction between the chains.

Algorithm 5: A two-scale coupled MCMC kernel for Half- $t(\nu)$ priors.

Input: Current states $C_t^{(i)} := (\beta_t^{(i)}, \eta_t^{(i)}, (\sigma_t^{(i)})^2, \xi_t^{(i)}) \in \mathbb{R}^p \times \mathbb{R}_{>0}^p \times \mathbb{R}_{>0} \times \mathbb{R}_{>0}$ for chains $i = 1, 2$, metric d on $\mathbb{R}^p \times \mathbb{R}_{>0}^p \times \mathbb{R}_{>0} \times \mathbb{R}_{>0}$, threshold $d_{threshold} \geq 0$.

if $C_t^{(1)} = C_t^{(2)}$ **then** Sample $C_{t+1}^{(1)}|C_t^{(1)}$ using Algorithm 1 and set $C_{t+1}^{(2)} = C_{t+1}^{(1)}$.

else

1. Calculate (or approximate) $d(C_t^{(1)}, C_t^{(2)})$.

if $d(C_t^{(1)}, C_t^{(2)}) \leq d_{threshold}$ **then**

| Sample $(\eta_{t+1}^{(1)}, \eta_{t+1}^{(2)})|C_t^{(1)}, C_t^{(2)}$ component-wise using Algorithm 4.

else

| Sample $(\eta_{t+1}^{(1)}, \eta_{t+1}^{(2)})|C_t^{(1)}, C_t^{(2)}$ component-wise using Algorithm 6.

2. Sample $((\xi_{t+1}^{(1)}, (\sigma_{t+1}^{(1)})^2, \beta_{t+1}^{(1)}), (\xi_{t+1}^{(2)}, (\sigma_{t+1}^{(2)})^2, \beta_{t+1}^{(2)})$ given $\eta_{t+1}^{(1)}, \eta_{t+1}^{(2)}$ as in Steps (2)(a – c) of Algorithm 3.

return $(C_{t+1}^{(1)}, C_{t+1}^{(2)})$.

Algorithm 6: Coupled Slice Sampler for Half- $t(\nu)$ priors with common random numbers.

Input: $\eta_{j,t}^{(1)}, \eta_{j,t}^{(2)}, m_{j,t}^{(1)} := \frac{\xi_t^{(1)}(\beta_{j,t}^{(1)})^2}{2(\sigma_t^{(1)})^2}, m_{j,t}^{(2)} := \frac{\xi_t^{(2)}(\beta_{j,t}^{(2)})^2}{2(\sigma_t^{(2)})^2} > 0$.

1. Sample $W_j^{crn} \sim \text{Uniform}(0, 1)$ and set $U_{j,*}^{(i)} = W_j^{crn}(1 + \nu\eta_{j,t}^{(i)})^{-\frac{\nu+1}{2}}$ for $i = 1, 2$.
2. Sample $V_j^{crn} \sim \text{Uniform}(0, 1)$ and set $\eta_{j,t+1}^{(i)} := \frac{1}{m_j^{(i)}}\gamma_s^{-1}\left(\gamma_s(m_{j,t}^{(i)}T_{j,*}^{(i)})V_j^{crn}\right)$ for $i = 1, 2$, where $T_{j,*}^{(i)}$, s and γ_s are defined as in the slice sampler of Algorithm 2.

return $(\eta_{j,t+1}^{(1)}, \eta_{j,t+1}^{(2)})$.

Choice and calculation of metric. Our chosen metric d on $\mathbb{R}^p \times \mathbb{R}_{>0}^p \times \mathbb{R}_{>0} \times \mathbb{R}_{>0}$ is

$$d(C_t^{(1)}, C_t^{(2)}) = \mathbb{P}_{\text{Algo(4)}} \left(\eta_{t+1}^{(1)} \neq \eta_{t+1}^{(2)} | C_t^{(1)}, C_t^{(2)} \right), \quad (10)$$

where $\mathbb{P}_{\text{Algo(4)}}$ is calculated under the slice sampler in Algorithm 4. Under this metric d , chains are close when $\mathbb{P}_{\text{Algo(4)}}(\eta_{t+1}^{(1)} = \eta_{t+1}^{(2)} | C_t^{(1)}, C_t^{(2)}) \geq 1 - d_{\text{threshold}}$. Precisely then our two-scale coupling applies Algorithm 4 at the coupled slice sampling step, such that the vectors $\eta_{t+1}^{(1)}$ and $\eta_{t+1}^{(2)}$ can exactly meet with probability greater than or equal to $1 - d_{\text{threshold}}$. Notice that once we manage to make $\eta_{t+1}^{(1)}$ and $\eta_{t+1}^{(2)}$ coincide (when scalars $\xi_{t+1}^{(1)}$ and $\xi_{t+1}^{(2)}$, and scalars $\sigma_{t+1}^{(1)}$ and $\sigma_{t+1}^{(2)}$ have also met), then the entire chains will meet at the next iteration.

We next consider methods to approximate this metric at a reasonably low cost.

1. We can directly form the Monte Carlo based estimate

$$\widehat{d}_R^{(1)}(C_t^{(1)}, C_t^{(2)}) = \frac{1}{R} \sum_{r=1}^R \mathbb{1}\{\tilde{\eta}_{t+1}^{(1),r} \neq \tilde{\eta}_{t+1}^{(2),r}\}, \quad (11)$$

where $(\tilde{\eta}_{t+1}^{(1),r}, \tilde{\eta}_{t+1}^{(2),r})$ are sampled independently for $r = 1, \dots, R$ using Algorithm 4.

2. As the coupling in Algorithm 4 is independent component-wise, we have

$$\begin{aligned} d(C_t^{(1)}, C_t^{(2)}) &= 1 - \mathbb{P}_{\text{Algo(4)}} \left(\eta_{t+1}^{(1)} = \eta_{t+1}^{(2)} | C_t^{(1)}, C_t^{(2)} \right) \\ &= 1 - \prod_{j=1}^p \mathbb{P}_{\text{Algo(4)}} \left(\eta_{j,t+1}^{(1)} = \eta_{j,t+1}^{(2)} | \eta_{j,t}^{(1)}, \eta_{j,t}^{(2)}, m_{j,t}^{(1)}, m_{j,t}^{(2)} \right), \end{aligned} \quad (12)$$

where $m_{j,t}^{(i)} = \xi_t^{(i)}(\beta_{j,t}^{(i)})^2 / (2(\sigma_t^{(i)})^2)$. We can calculate $d(C_t^{(1)}, C_t^{(2)})$ by evaluating the one-dimensional integrals in Equation (12) using numerical integration or analytically.

3. We can form Rao-Blackwellized estimates by combining Monte Carlo with analytical calculations of integrals. We can obtain the estimate

$$\widehat{d}_R^{(2)}(C_t^{(1)}, C_t^{(2)}) = 1 - \prod_{j=1}^p \left(\frac{1}{R} \sum_{r=1}^R \mathbb{P}_{\text{max}} \left(\eta_{j,t+1}^{(1)} = \eta_{j,t+1}^{(2)} \middle| U_{j,r}^{(1)}, U_{j,r}^{(2)}, m_{j,t}^{(1)}, m_{j,t}^{(2)} \right) \right), \quad (13)$$

where $(U_{j,r}^{(1)}, U_{j,r}^{(2)})$ are sampled independently for $r = 1, \dots, R$ using Algorithm 4 and each $\mathbb{P}_{\text{max}}(\eta_{j,t+1}^{(1)} = \eta_{j,t+1}^{(2)} | U_{j,r}^{(1)}, U_{j,r}^{(2)}, m_{j,t}^{(1)}, m_{j,t}^{(2)})$ is calculated analytically.

Further metric calculation details are in Appendix B. For a number of samples R , estimates (11) and (13) both have computation cost of order pR . Compared to the estimate in (11), the estimate in (13) has lower variance and faster numerical run-times as it only involves sampling uniformly distributed random numbers. It suffices to choose a small number of samples R , and often we take $R = 1$. Note that it is not necessary to accurately estimate $d(C_t^{(1)}, C_t^{(2)})$, as we are only interested in checking how that distance compares to a fixed threshold $d_{\text{threshold}} \in [0, 1]$. Often $(d(C_t^{(1)}, C_t^{(2)}))_{t \geq 0}$ trajectories initially take values close to 1, and then sharply drop to values close to 0. This leads to the estimates in (11) and (13) having low variance even for small number of samples R . Henceforth, we will use the estimate in (13) in our experiments with two-scale couplings, unless specified otherwise.

Comparison with other metrics. Figure 4 plots $d(C_t^{(1)}, C_t^{(2)})$ alongside the L_1 metric and the log-transformed L_1 metric on parameters $m_{j,t}^{(i)}$ as in Equation (12). It is based on one trajectory of our two-scale coupled chain under common random numbers (Algorithm 5 with $d_{\text{threshold}} = 0$), for a synthetic dataset generated as per Section 3.1 targeting the Horseshoe posterior ($\nu = 1$) with $a_0 = b_0 = 1$. Figure 4 shows

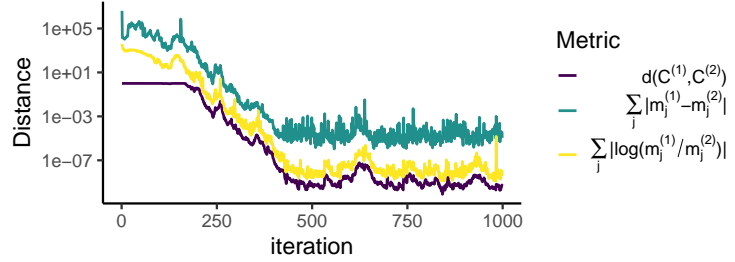


Figure 4: Metric trajectories for the posterior associated with a Horseshoe prior under common random numbers coupling with $n = 100$, $p = 1000$, $s = 10$ and $\sigma_* = 0.5$.

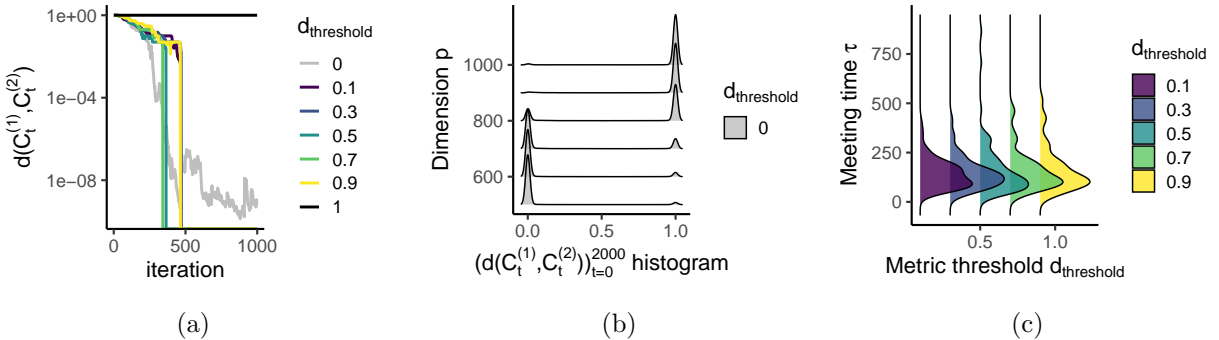


Figure 5: Two-scale coupling algorithm performance for the Horseshoe prior under different values of $d_{threshold}$. Unless specified otherwise, $n = 100$, $p = 500$, $s = 20$ and $\sigma_* = 2$.

that $d(C_t^{(1)}, C_t^{(2)})$ is bounded above by both the L_1 metric and the L_1 metric between the logarithms of $m_j^{(1)}, m_j^{(2)}$. Therefore, we could consider the capped L_1 metric ($\min\{\sum_j |m_{j,t}^{(1)} - m_{j,t}^{(2)}|, 1\}$) or the capped L_1 metric on the logs ($\min\{\sum_j |\log(|m_{j,t}^{(1)} / m_{j,t}^{(2)}|)|, 1\}$) to obtain upper bounds on d . Finding metrics which are easily calculable and accurately approximate or bound d could be investigated further and may prove valuable for theoretical analysis of our coupling algorithms.

Choice of metric threshold. For metric d from Equation (10), we now consider the choice of threshold $d_{threshold} \in [0, 1]$. When $d_{threshold} = 1$, we always apply the maximal coupling slice sampler (Algorithm 4). This corresponds to the one-scale coupling of Algorithm 3. When $d_{threshold} = 0$, we always apply the common random numbers slice sampler (Algorithm 6). Then the chains $C_t^{(1)}, C_t^{(2)}$ may come arbitrarily close with respect to metric d , but will never exactly meet. Figure 5 highlights the impact of $d_{threshold}$. It is based on 100 replicate simulations of 1-Lag coupled Markov chains, where the synthetic datasets are generated as per Section 3.1 and we target the Horseshoe posterior ($\nu = 1$) with $a_0 = b_0 = 1$. For different values of $d_{threshold}$, Figure 5a shows averaged trajectories $(d(C_t^{(1)}, C_t^{(2)}))_{t \geq 0}$. When $d_{threshold} = 1$ (one-scale coupling), metric $d(C_t^{(1)}, C_t^{(2)})$ remains near 1, and when $d_{threshold} = 0$ (common random numbers coupling) metric $d(C_t^{(1)}, C_t^{(2)})$ gets very close to but does not exactly equal 0. For all values of the threshold shown, the chains exactly meet and $d(C_t^{(1)}, C_t^{(2)})$ reaches zero at similar times. Figure 5b considers higher dimensional settings. It plots the histograms of $(d(C_t^{(1)}, C_t^{(2)}))_{t=1}^{2000}$ when $d_{threshold} = 0$. The histograms show that $d(C_t^{(1)}, C_t^{(2)})$ takes values close to either 1 or 0 for different dimensions p . This appears to be a cutoff phenomenon, as in Diaconis [1996], and explains why different threshold values sufficiently away from 0 and 1 give similar meeting times. Figure 5c shows that different thresholds give similar meeting times for the Horseshoe.

Computation Cost. We consider the computation cost of each step of Algorithm 5. When $C_t^{(1)} \neq C_t^{(2)}$, Step (1) of Algorithm 5 involves calculating a distance estimate and sampling from a coupled slice sampling

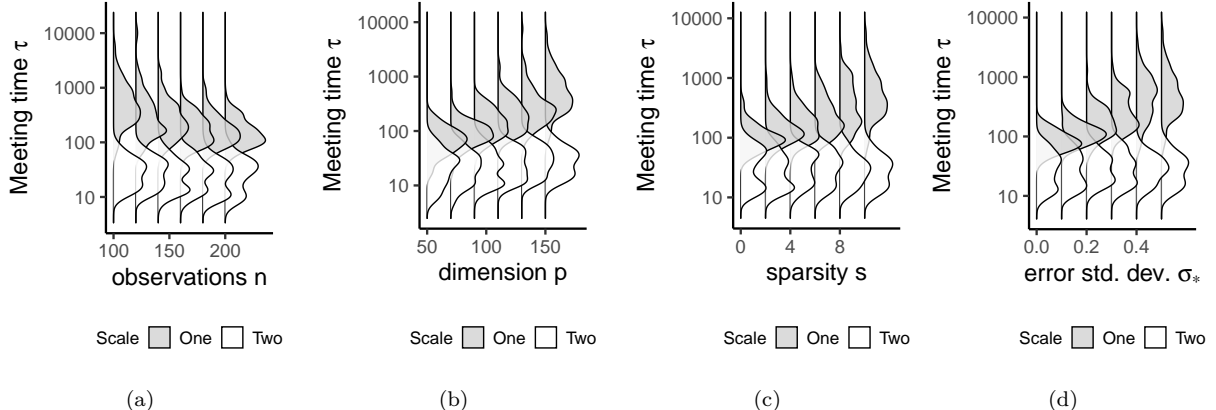


Figure 6: Meeting times for posteriors from the Horseshoe prior under one-scale and two-scale coupling algorithms. Unless specified otherwise, $n = 100$, $p = 150$, $s = 10$, $\sigma_* = 0.5$

kernel. Calculating the distance estimate involves sampling $2pR$ uniforms and has $\mathcal{O}(p)$ cost. Coupled slice sampling with maximal couplings (Algorithm 4) or common random numbers (Algorithm 6) both have expected or deterministic cost $\mathcal{O}(p)$. Steps (2)(a–b) of Algorithm 5 use maximal couplings, which have twice the cost in expectation as the corresponding steps of Algorithm 1. Step (2)(c) uses common random numbers, which has twice the cost deterministically as the corresponding step of Algorithm 1. Overall, Algorithm 5 has twice the $\mathcal{O}(n^2p)$ cost of the kernel in Algorithm 1.

Simulations. We consider the performance of Algorithm 5 on synthetic datasets. The synthetic datasets are generated as per Section 3.1. We target the Horseshoe posterior ($\nu = 1$) with $a_0 = b_0 = 1$. Figure 6 shows the meeting times τ of a 1-Lag coupled Markov chain for both the one-scale coupling of Algorithm 3 and the two-scale coupling of Algorithm 5 with $R = 1$ and $d_{threshold} = 0.5$. For both coupled kernels, we initialize at the prior distribution (Equation (2)) independently for chains $i = 1, 2$. For the ξ updates, we use a Metropolis–Hastings step-size of $\sigma_{MH} = 0.8$. Each sub-figure plots kernel density estimates of τ against each parameter n, p, s, σ_* respectively, based on 100 independent iterations. All sub-figures show that the two-scale coupling has orders of magnitude smaller coupling times compared to the one-scale coupling when the number of observations is low, or the dimension, sparsity parameter and true error standard deviation are high.

3.3 Computational and statistical impact of degree of freedom ν

In this section, we investigate the impact of the degree of freedom $\nu \geq 1$ for Half- $t(\nu)$ priors. Higher degrees of freedom ν corresponds to priors on β which have stronger shrinkage towards zero (Proposition 2.1). We consider meeting times of the two-scale coupling algorithm in Section 3.2 and the statistical performance of the posteriors.

Coupled MCMC simulations. We consider the performance of coupled MCMC with Half- $t(\nu)$ priors under the two-scale coupling of Algorithm 5 (with $R = 1$ and $d_{threshold} = 0.5$) on synthetic datasets. The synthetic datasets are generated as per Figure 3 of Section 3.1. We initialize both chains independently at the prior distribution (Equation (2)). For the ξ updates, we use a Metropolis–Hastings step-size of $\sigma_{MH} = 0.8$. Figures 7 and 8 are based on 20 independent iterations for different degrees of freedom $\nu \in [1, 2]$.

Figure 7a plots averaged trajectories $d(C_t^{(1)}, C_t^{(2)})_{t \geq 0}$ under common random numbers coupling ($d_{threshold} = 0$). It highlights that using higher degrees of freedom ν allow the pair of chains to get closer with respect to metric d quickly. This leads to fast coupling times for higher values of ν , as shown in Figures 7b and 7c. Figure 7b plots meeting times τ of 1-lag coupled Markov chains against dimension, showing that higher values of ν can significantly improve scalability. The case $\nu = 2$ is further highlighted in Figure 7c, showing stable coupling times with increasing dimensions.

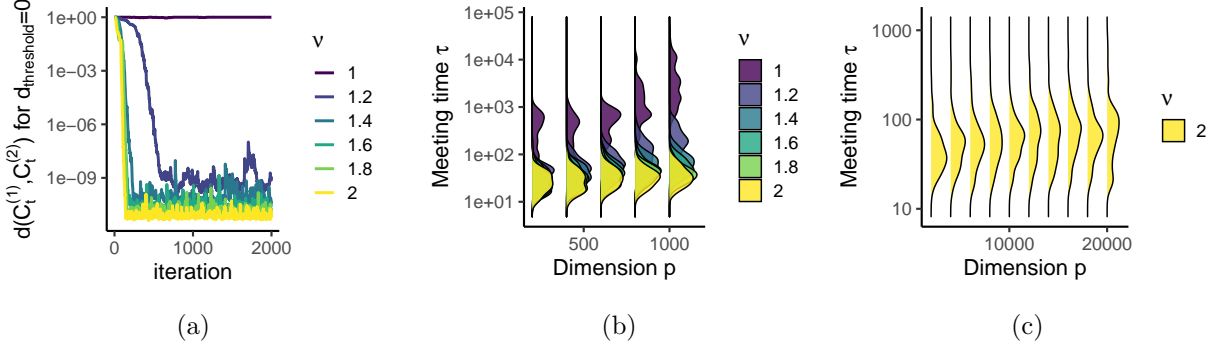


Figure 7: Meeting times for Half- $t(\nu)$ priors under the two-scale coupling algorithm. Unless specified otherwise, $n = 100$, $p = 1000$, $s = 20$ and $\sigma_* = 2$.

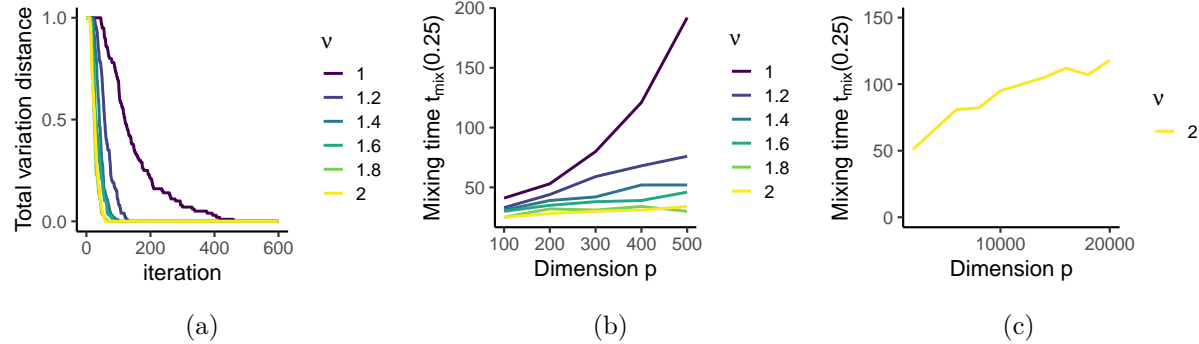


Figure 8: L -lag total variation bounds for Half- $t(\nu)$ priors under the two-scale coupling algorithm. Unless specified otherwise, $n = 100$, $p = 500$, $s = 20$ and $\sigma_* = 2$.

Figure 8 plots upper bounds on total variation and mixing times using L -lag couplings [Biswas et al., 2019]. Figure 8a plots total variation bounds with $L = 500$, showing faster convergence upper bounds for higher values of ν . Figure 8b plots the corresponding upper bounds on mixing time against dimension, showing that higher values of ν can give more favorable mixing time upper bounds. The case $\nu = 2$ is further highlighted in Figure 8c with $L = 500$, showing stable mixing time upper bounds in high dimensions.

Overall, Figures 7 and 8 indicate that even a small increase in the degree of freedom $\nu > 1$ compared to the Horseshoe ($\nu = 1$) can lead to orders of magnitude computational improvements through shorter coupling times and faster convergence upper bounds.

Statistical performance simulations. We consider the statistical performance of Bayesian shrinkage regression with Half- $t(\nu)$ priors on synthetic datasets. The synthetic datasets are generated as per Figure 3 of Section 3.1. We use the blocked Gibbs sampler of Algorithm 1 to draw samples from the posteriors corresponding to different degrees of freedom ν , by simulating chains of length 1000 with burn-in based on the L -lag total variation bounds from Figure 8a: a burn-in of 300 steps for $\nu \geq 1.2$ and of 600 steps for $\nu = 1$. Figures 9 and 10 are then generated using 100 independent chains for each value of ν .

Figure 9 shows component-wise densities for Half- $t(\nu)$ priors. It highlights how different values of $\nu \geq 1$ impact the posterior distribution. For larger signals (Figure 9a), the component-wise posteriors are all uni-modal about the true signal for $\nu \in [1, 2]$. For medium-sized signals (Figure 9b), they are bi-modal about the true signal and about zero, with greater weight at zero for higher values of $\nu \in [1, 2]$ corresponding to more concentrated priors. Smaller signals close to zero are not identified (Figure 9c), with the component-wise posteriors all being uni-modal about zero for $\nu \geq 1$. For null signals (Figure 9d), the component-wise posteriors are all uni-modal about zero for $\nu \geq 1$.

Figure 10 highlights the statistical performance of Half- $t(\nu)$ priors under different values of $\nu \geq 1$. Figures 10a and 10b show similar mean squared error (MSE) and frequentist coverage of highest posterior density (HPD)

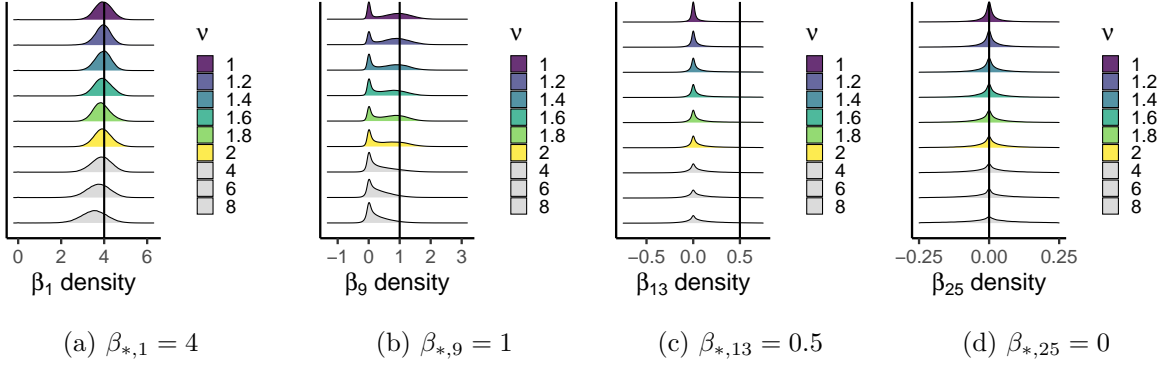


Figure 9: Posterior densities for Half- $t(\nu)$ priors with $n = 100, p = 500, s = 20, \sigma_* = 2$.

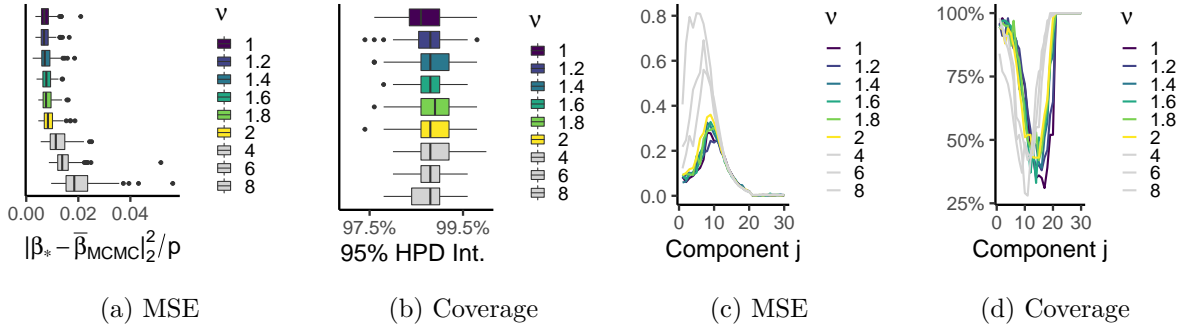


Figure 10: Statistical performance of Half- $t(\nu)$ priors with $n = 100, p = 500, s = 20, \sigma_* = 2$.

intervals for different values of $\nu \in [1, 2]$. For a fixed synthetic dataset, the MSE in Figure 10a is calculated as $\|\beta_* - \bar{\beta}_{MCMC}\|_2^2/p$ where $\bar{\beta}_{MCMC} = \sum_{t=\text{burn-in}+1}^{\text{burn-in}+1000} \beta_t/1000$ is the time-averaged MCMC estimator from a Markov chain. For a fixed synthetic dataset, coverage is calculated by first calculating univariate 95%-HPD intervals $I_{j,HPD}$ for each component β_j , and then calculating the proportion $\sum_{j=1}^p \mathbb{1}\{\beta_{*,j} \in I_{j,HPD}\}/p$ of such HPD intervals which contain true signal components $\beta_{*,j}$. The error bars for Figures 10a and 10b are generated by simulating synthetic datasets independently 100 times and each time calculating the corresponding MSE and coverage from a Markov chain for different values of $\nu \in [1, 2]$.

Figures 10c and 10d present the component-wise MSE and frequentist coverage of HPD intervals for different values of $\nu \geq 1$ respectively. For each component j , Figures 10c and 10d plots $(\beta_{*,j} - \bar{\beta}_{MCMC,j})^2$ and $\mathbb{1}\{\beta_{*,j} \in I_{j,HPD}\}$ respectively averaged over 100 independent synthetic datasets, both showing similar performance for different components β_j . With $\nu \in [1, 2]$, we observe good statistical performance for components j corresponding to large or medium-sized signals $\beta_{*,j}$, or $j > 20$ corresponding to null signals $\beta_{*,j} = 0$ (as per the density plots of Figures 9a, 9b or 9d respectively), and worse statistical performance for components j corresponding to small signals $\beta_{*,j}$ (as per the density plot of Figure 9c).

The grey plots in Figures 9 and 10 show that much larger $\nu \in \{4, 6, 8\}$ can lead to higher MSE (Figure 10a), as the corresponding posteriors are strongly concentrated about zero and less able to identify non-null signals (as per Figures 9b and 10a).

Overall, Figures 9 and 10 illustrate that Half- $t(\nu)$ priors with degrees of freedom $\nu \in [1, 2]$ can result in comparable statistical performance in high dimensions, with the performance visibly deteriorating only for much larger values of ν .

4 Results on a GWAS dataset

Section 3.3 suggests that Half- $t(\nu)$ priors with higher degrees of freedom $\nu > 1$ can give similar statistical performance to the Horseshoe ($\nu = 1$), whilst allowing orders of magnitude computational improvements.

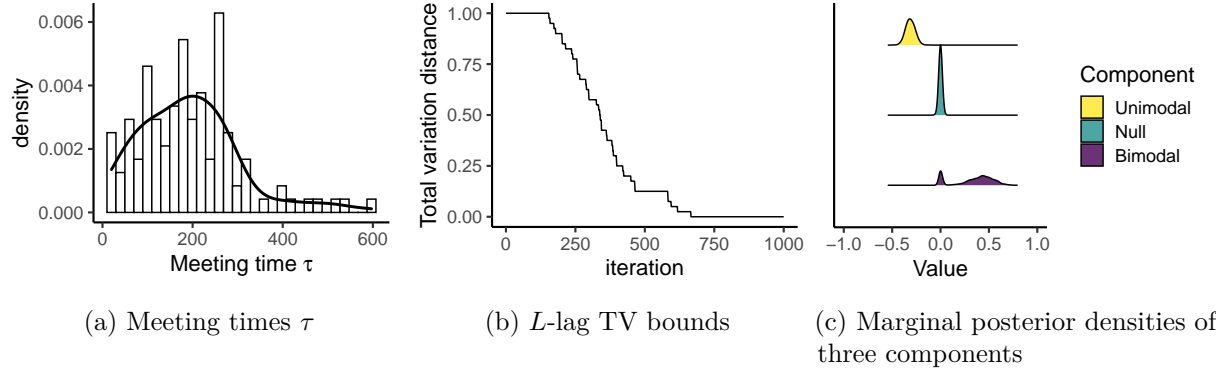


Figure 11: Coupled Bayesian shrinkage regression with Half- $t(2)$ prior on a GWAS dataset.

Motivated by this insight, we apply our algorithms to a maize genome-wide association study (GWAS) dataset [Romay et al., 2013, Liu et al., 2016, Zeng and Zhou, 2017, Johndrow et al., 2020]. There are $n = 2,266$ observations corresponding to average number of days taken for silk emergence in different maize lines, and $p = 98,385$ covariates corresponding to single nucleotide polymorphisms (SNPs) in the genome. For this dataset, we target the Half- $t(2)$ posterior with $a_0 = b_0 = 1$. We use the two-scale coupling of Algorithm 5 with $R = 1$ and $d_{threshold} = 0.5$, and initialize both chains independently at the prior distribution. For the ξ updates, we use a Metropolis–Hastings step-size of $\sigma_{\text{MH}} = 0.8$. Figure 11 shows results based on 100 independent coupled chains. Figure 11a plots meetings times of the coupled chain, showing short meeting times which thereby allow fast parallel computation through unbiased MCMC. Figure 11b plots total variation upper bounds using L -lag couplings with $L = 750$, highlighting fast convergence of the single Markov chain. Figure 11c shows componentwise densities based on one trajectory of a single Markov chain of length 1,000 iterations with a burn-in of 700 iterations (as per the burn-in guidance from Figure 11b). The density plots show marginal posteriors corresponding to a null unimodal (the first covariate), a non-zero unimodal (the covariate with the largest negative posterior mean), and a bimodal distribution (the covariate with the largest positive posterior mean). Overall, this GWAS example shows the favorable performance of our coupling algorithms in practical high-dimensional settings.

We note that the MCMC run-time per iteration may still be significant in such large-scale settings. For this GWAS example on a 2015 Macbook Pro, each iteration of the coupled chain takes approximately 1 minute, and running one coupled chain until meeting can take one to two days. This run-time is dominated by the calculation of the weighted matrix cross-product $X\text{Diag}(\eta)^{-1}X^T$, which has $\mathcal{O}(n^2p)$ cost. In other cases with smaller n such that $n^2 \leq p$, the run-time may be dominated by other parts of the algorithm.

5 Discussion

We have introduced coupled Gibbs samplers for Bayesian shrinkage regression with Half- $t(\nu)$ priors. Our two-scale coupling is operational in realistic high-dimensional settings, including a GWAS setting with $n \approx 2,000, p \approx 100,000$ in Section 4.

Firstly, our work participates in an effort to apply MCMC algorithms and coupling techniques to large problems. The problems considered here are orders of magnitude larger in dimension than the related experiments on Bayesian variable selection in Jacob et al. [2020]. This relates to some questions raised by e.g. the comments of Lee et al. [2020] and Paulin [2020] in the discussion of Jacob et al. [2020]. Secondly, we have applied L -lag couplings [Biswas et al., 2019] to obtain upper bounds on the total variation distance between the chain at finite iterations and its stationary distribution. This allows empirical investigations of the Markov chain mixing times with the inputs of the problem, including number of observations, number of covariates, signal to noise ratio and sparsity. We find that such coupling techniques constitute a convenient, non-asymptotic tool to monitor the performance of MCMC algorithms. Thirdly, we observe that Half- $t(\nu)$ priors with degrees of freedom ν higher than one give similar statistical estimation performance than the Horseshoe whilst providing significant computational advantages. This contributes towards the discussion on

the impact of the prior on the trade-off between statistical estimation and computational feasibility, in the setting of high-dimensional Bayesian regression.

Some open questions arise from our work:

1. *Convergence of the blocked Gibbs sampler.* Fast coupling times suggest our blocked Gibbs sampler converges quickly in high dimensions. This motivates studying the convergence complexity of the Markov chain to analytically understand convergence in terms of features of the data generating process and the choice of prior. Our Lyapunov function in Proposition 2.3 and the two-scale coupled kernel in Algorithm 5 which empirically gives rapid meetings and shows little dependence on dimension may prove useful for such analysis. Our initial work in this area suggests that finding a convenient metric that gives sharp bounds on the metric d used here, while simultaneously being amenable to theoretical analysis, will be a key step.
2. *Alternative coupling algorithms.* Alternative couplings (for example, combinations of reflection, common random numbers, component-wise and full vector couplings) may give shorter coupling times for the Horseshoe prior. This may allow the Horseshoe prior to remain competitive with Half- $t(\nu)$ priors with higher degrees of freedom. We emphasize that nothing we have done thus far suggests that alternative coupling strategies would give faster meetings for the Horseshoe, but certainly cannot rule out this possibility based only on the behavior of the couplings considered here.
3. *Interplay between posterior concentration and MCMC convergence.* For Bayesian regression with spike-and-slab priors, Yang et al. [2016] and Atchadé [2019] have shown that posterior contraction can aid the convergence of MCMC in high dimensions. The performance of our coupling algorithms motivates similar investigations for continuous shrinkage priors.

Acknowledgement. The authors thank Professors Xiaolei Liu and Xiang Zhou for sharing the Maize GWAS data. Niloy Biswas thanks Yves F. Atchadé for a helpful discussion. Anirban Bhattacharya gratefully acknowledges support from an NSF CAREER award (DMS-1653404). Pierre E. Jacob gratefully acknowledges support by the National Science Foundation through grants DMS-1712872 and DMS-1844695. The GWAS simulations in this article were run on the FASRC Cannon cluster supported by the FAS Division of Science Research Computing Group at Harvard University.

References

M. Abramowitz. *Handbook of Mathematical Functions, With Formulas, Graphs, and Mathematical Tables*,. Dover Publications, Inc., USA, 1974. ISBN 0486612724. 4, 22, 23, 26

Y. F. Atchadé. Approximate spectral gaps for Markov chains mixing times in high dimensions. *arXiv preprint arXiv:1903.11745*, 2019. 18

A. Bhadra, J. Datta, N. G. Polson, and B. Willard. Lasso meets Horseshoe: A survey. *Statistical Science*, 34(3):405–427, 2019. 2

A. Bhattacharya, D. Pati, N. S. Pillai, and D. B. Dunson. Dirichlet–Laplace priors for optimal shrinkage. *Journal of the American Statistical Association*, 110(512):1479–1490, 2015. doi: 10.1080/01621459.2014.960967. URL <https://doi.org/10.1080/01621459.2014.960967>. 5, 7

A. Bhattacharya, A. Chakraborty, and B. K. Mallick. Fast sampling with Gaussian scale mixture priors in high-dimensional regression. *Biometrika*, 103(4):985–991, 10 2016. ISSN 0006-3444. doi: 10.1093/biomet/asw042. URL <https://doi.org/10.1093/biomet/asw042>. 5, 35

S. K. Bhattacharya, K. Khare, and S. Pal. Geometric ergodicity of gibbs samplers for the horseshoe and its regularized variants. *arXiv preprint arXiv:2101.00366*, 2021. 3

N. Biswas, P. E. Jacob, and P. Vanetti. Estimating convergence of Markov chains with L-lag couplings. In *Advances in Neural Information Processing Systems*, pages 7389–7399, 2019. 2, 9, 15, 17

N. Bou-Rabee and A. Eberle. Two-scale coupling for preconditioned Hamiltonian Monte Carlo in infinite dimensions. *Stochastics and Partial Differential Equations: Analysis and Computations*, 2020. doi: 10.1007/s40072-020-00175-6. URL <https://doi.org/10.1007/s40072-020-00175-6>. 10

N. Bou-Rabee and J. M. Sanz-Serna. Geometric integrators and the Hamiltonian Monte Carlo method. *Acta Numerica*, 27:113–206, 2018. doi: 10.1017/S0962492917000101. 5

C. M. Carvalho, N. G. Polson, and J. G. Scott. Handling sparsity via the horseshoe. In *Proceedings of Machine Learning Research*, volume 5, pages 73–80. PMLR, 2009. URL <http://proceedings.mlr.press/v5/carvalho09a.html>. 2

C. M. Carvalho, N. G. Polson, and J. G. Scott. The horseshoe estimator for sparse signals. *Biometrika*, 97(2):465–480, 2010. ISSN 00063444. URL <http://www.jstor.org/stable/25734098>. 2, 5

P. Diaconis. The cutoff phenomenon in finite Markov chains. *Proceedings of the National Academy of Sciences*, 93(4):1659–1664, 1996. ISSN 0027-8424. doi: 10.1073/pnas.93.4.1659. URL <https://www.pnas.org/content/93/4/1659>. 13

A. Gelman. Prior distributions for variance parameters in hierarchical models (comment on article by Browne and Draper). *Bayesian Anal.*, 1(3):515–534, 09 2006. doi: 10.1214/06-BA117A. URL <https://doi.org/10.1214/06-BA117A>. 2

P. Ghosh and A. Chakrabarti. Asymptotic optimality of one-group shrinkage priors in sparse high-dimensional problems. *Bayesian Anal.*, 12(4):1133–1161, 12 2017. doi: 10.1214/16-BA1029. URL <https://doi.org/10.1214/16-BA1029>. 2

P. W. Glynn and C.-h. Rhee. Exact estimation for Markov chain equilibrium expectations. *Journal of Applied Probability*, 51(A):377–389, 2014. 2

J. E. Griffin and P. J. Brown. Inference with Normal-Gamma prior distributions in regression problems. *Bayesian Anal.*, 5(1):171–188, 03 2010. doi: 10.1214/10-BA507. URL <https://doi.org/10.1214/10-BA507>. 7

A. E. Hoerl and R. W. Kennard. Ridge regression: Biased estimation for nonorthogonal problems. *Technometrics*, 12(1):55–67, 1970. doi: 10.1080/00401706.1970.10488634. URL <https://www.tandfonline.com/doi/abs/10.1080/00401706.1970.10488634>. 8, 24

P. E. Jacob, J. O’Leary, and Y. F. Atchadé. Unbiased Markov chain Monte Carlo methods with couplings. *Journal of the Royal Statistical Society: Series B (Statistical Methodology)*, 82(3):543–600, 2020. doi: 10.1111/rssb.12336. URL <https://rss.onlinelibrary.wiley.com/doi/abs/10.1111/rssb.12336>. 2, 3, 9, 17

S. Jarner and G. Roberts. Convergence of heavy-tailed Monte Carlo Markov Chain algorithms. *Scandinavian Journal of Statistics*, 34:781–815, 02 2007. doi: 10.1111/j.1467-9469.2007.00557.x. 5

S. F. Jarner and R. L. Tweedie. Necessary conditions for geometric and polynomial ergodicity of random-walk-type. *Bernoulli*, 9(4):559–578, 08 2003. doi: 10.3150/bj/1066223269. URL <https://doi.org/10.3150/bj/1066223269>. 5

J. Johndrow, P. Orenstein, and A. Bhattacharya. Scalable approximate MCMC algorithms for the horseshoe prior. *Journal of Machine Learning Research*, 21(73):1–61, 2020. URL <http://jmlr.org/papers/v21/19-536.html>. 3, 5, 7, 8, 10, 17, 27, 37

L. T. Johnson and C. J. Geyer. Variable transformation to obtain geometric ergodicity in the random-walk Metropolis algorithm. *Ann. Statist.*, 40(6):3050–3076, 12 2012. doi: 10.1214/12-AOS1048. URL <https://doi.org/10.1214/12-AOS1048>. 5

V. E. Johnson. Studying convergence of Markov chain Monte Carlo algorithms using coupled sample paths. *Journal of the American Statistical Association*, 91(433):154–166, 1996. 2

V. E. Johnson. A coupling-regeneration scheme for diagnosing convergence in Markov chain Monte Carlo algorithms. *Journal of the American Statistical Association*, 93(441):238–248, 1998. [2](#), [9](#)

V. E. Johnson and D. Rossell. Bayesian model selection in high-dimensional settings. *Journal of the American Statistical Association*, 107(498):649–660, 2012. doi: 10.1080/01621459.2012.682536. URL <https://doi.org/10.1080/01621459.2012.682536>. [2](#)

K. Khare and J. P. Hobert. Geometric ergodicity of the Bayesian lasso. *Electron. J. Statist.*, 7:2150–2163, 2013. doi: 10.1214/13-EJS841. URL <https://doi.org/10.1214/13-EJS841>. [3](#), [7](#)

A. Lee, S. S. Singh, and M. Vihola. Comment on ‘Unbiased Markov chain Monte Carlo with couplings’ by Jacob, O’leary and Atchadé. *Journal of the Royal Statistical Society: Series B (Statistical Methodology)*, 2020. [17](#)

X. Liu, M. Huang, B. Fan, E. S. Buckler, and Z. Zhang. Iterative usage of fixed and random effect models for powerful and efficient genome-wide association studies. *PLOS Genetics*, 12(2):1–24, 02 2016. doi: 10.1371/journal.pgen.1005767. URL <https://doi.org/10.1371/journal.pgen.1005767>. [17](#)

S. Livingstone, M. Betancourt, S. Byrne, and M. Girolami. On the geometric ergodicity of Hamiltonian Monte Carlo. *Bernoulli*, 25(4A):3109–3138, 11 2019a. doi: 10.3150/18-BEJ1083. URL <https://doi.org/10.3150/18-BEJ1083>. [5](#)

S. Livingstone, M. F. Faulkner, and G. O. Roberts. Kinetic energy choice in Hamiltonian/hybrid Monte Carlo. *Biometrika*, 106(2):303–319, 2019b. [5](#)

E. Makalic and D. F. Schmidt. A simple sampler for the horseshoe estimator. *IEEE Signal Processing Letters*, 23(1):179–182, 2016. [5](#)

S. P. Meyn and R. L. Tweedie. *Markov chains and stochastic stability*. Springer, 1993. [7](#)

S. Pal and K. Khare. Geometric ergodicity for Bayesian shrinkage models. *Electron. J. Statist.*, 8(1):604–645, 2014. doi: 10.1214/14-EJS896. URL <https://doi.org/10.1214/14-EJS896>. [3](#), [7](#)

T. Park and G. Casella. The Bayesian lasso. *Journal of the American Statistical Association*, 103(482):681–686, 2008. doi: 10.1198/016214508000000337. URL <https://doi.org/10.1198/016214508000000337>. [5](#)

D. Paulin. Comment on ‘Unbiased Markov chain Monte Carlo with couplings’ by Jacob, O’leary and Atchadé. *Journal of the Royal Statistical Society: Series B (Statistical Methodology)*, 2020. [17](#)

N. G. Polson and J. G. Scott. On the half-Cauchy prior for a global scale parameter. *Bayesian Analysis*, 7(4):887–902, 2012. [2](#)

N. G. Polson, J. G. Scott, and J. Windle. The Bayesian bridge. *Journal of the Royal Statistical Society: Series B (Statistical Methodology)*, 76(4):713–733, 2014. doi: 10.1111/rssb.12042. URL <https://rss.onlinelibrary.wiley.com/doi/abs/10.1111/rssb.12042>. [5](#)

Q. Qin and J. P. Hobert. Wasserstein-based methods for convergence complexity analysis of MCMC with applications. *arXiv preprint arXiv:1810.08826*, 2019. [8](#)

Q. Qin and J. P. Hobert. On the limitations of single-step drift and minorization in Markov chain convergence analysis. *arXiv preprint arXiv:2003.09555*, 2020. [8](#)

R Core Team. *R: A Language and Environment for Statistical Computing*. R Foundation for Statistical Computing, Vienna, Austria, 2013. URL <http://www.R-project.org/>. [3](#)

B. Rajaratnam and D. Sparks. MCMC-based inference in the era of big data: A fundamental analysis of the convergence complexity of high-dimensional chains. *arXiv preprint arXiv:1508.00947*, 2015. [8](#)

G. O. Roberts and J. S. Rosenthal. General state space Markov chains and MCMC algorithms. *Probability surveys*, 1:20–71, 2004. [7](#)

G. O. Roberts and R. L. Tweedie. Exponential convergence of Langevin distributions and their discrete approximations. *Bernoulli*, 2(4):341–363, 1996. ISSN 13507265. URL <http://www.jstor.org/stable/3318418>. 5

M. C. Romay, M. J. Millard, J. C. Glaubitz, J. A. Peiffer, K. L. Swarts, T. M. Casstevens, R. J. Elshire, C. B. Acharya, S. E. Mitchell, S. A. Flint-Garcia, M. D. McMullen, J. B. Holland, E. S. Buckler, and C. A. Gardner. Comprehensive genotyping of the USA national maize inbred seed bank. *Genome Biology*, 14(6):R55, 2013. doi: 10.1186/gb-2013-14-6-r55. URL <https://doi.org/10.1186/gb-2013-14-6-r55>. 17

J. S. Rosenthal. Minorization conditions and convergence rates for Markov chain Monte Carlo. *Journal of the American Statistical Association*, 90(430):558–566, 1995. ISSN 01621459. URL <http://www.jstor.org/stable/2291067>. 8

C. Sherlock, P. Fearnhead, and G. O. Roberts. The random walk Metropolis: Linking theory and practice through a case study. *Statist. Sci.*, 25(2):172–190, 05 2010. doi: 10.1214/10-STS327. URL <https://doi.org/10.1214/10-STS327>. 5

H. Thorisson. *Coupling, stationarity, and regeneration*. Springer, 2000. 9

R. Tibshirani. Regression shrinkage and selection via the lasso. *Journal of the Royal Statistical Society, Series B*, 58:267–288, 1994. 1

S. van der Pas, B. Szabó, and A. van der Vaart. Adaptive posterior contraction rates for the horseshoe. *Electron. J. Statist.*, 11(2):3196–3225, 2017. doi: 10.1214/17-EJS1316. URL <https://doi.org/10.1214/17-EJS1316>. 7

S. L. van der Pas, B. J. K. Kleijn, and A. W. van der Vaart. The horseshoe estimator: Posterior concentration around nearly black vectors. *Electron. J. Statist.*, 8(2):2585–2618, 2014. doi: 10.1214/14-EJS962. URL <https://doi.org/10.1214/14-EJS962>. 2

D. Vats and C. Knudson. Revisiting the Gelman–Rubin diagnostic. *Statistical Science (to appear)*, 2020. 1

D. Vats, J. M. Flegal, and G. L. Jones. Multivariate output analysis for Markov chain Monte Carlo. *Biometrika*, 106(2):321–337, 04 2019. ISSN 0006-3444. doi: 10.1093/biomet/asz002. URL <https://doi.org/10.1093/biomet/asz002>. 1

Y. Yang, M. J. Wainwright, and M. I. Jordan. On the computational complexity of high-dimensional Bayesian variable selection. *Ann. Statist.*, 44(6):2497–2532, 12 2016. doi: 10.1214/15-AOS1417. URL <https://doi.org/10.1214/15-AOS1417>. 18

P. Zeng and X. Zhou. Non-parametric genetic prediction of complex traits with latent Dirichlet process regression models. *Nature Communications*, 8(1):456, 2017. doi: 10.1038/s41467-017-00470-2. URL <https://doi.org/10.1038/s41467-017-00470-2>. 17

H. Zou and T. Hastie. Regularization and variable selection via the Elastic Net. *Journal of the Royal Statistical Society, Series B*, 67:301–320, 2005. 1

A Proofs

A.1 Marginal β prior and posterior densities

Proof of Proposition 2.1.

Marginal Prior on β . Let π_η denote the component-wise prior density of each η_j based on the Half- $t(\nu)$ distribution, and $\mathcal{N}(\cdot; \mu, \Sigma)$ the density of a multivariate Normal distribution with mean μ and Σ . It suffices to calculate the marginal prior for each β_j given ξ, σ^2 , by marginalizing over each η_j . We obtain,

$$\begin{aligned}
\pi(\beta_j | \xi, \sigma^2) &= \int_0^\infty \mathcal{N}\left(\beta_j; 0, \frac{\sigma^2}{\xi \eta_j}\right) \pi_\eta(\eta_j) d\eta_j \\
&\propto \int_0^\infty \frac{\sqrt{\xi \eta_j}}{\sqrt{2\pi\sigma^2}} \exp\left(-\frac{\xi \beta_j^2}{2\sigma^2} \eta_j\right) \frac{1}{\eta_j^{\frac{2-\nu}{2}} (1 + \nu \eta_j)^{\frac{\nu+1}{2}}} d\eta_j \\
&\propto \int_0^\infty \frac{1}{\eta_j^{\frac{1-\nu}{2}} (1 + \nu \eta_j)^{\frac{\nu+1}{2}}} \exp\left(-\frac{\xi \beta_j^2}{2\sigma^2} \eta_j\right) d\eta_j \\
&= \int_0^\infty \frac{1}{\left(\frac{t}{\nu}\right)^{\frac{1-\nu}{2}} (1+t)^{\frac{\nu+1}{2}}} \exp\left(-\frac{\xi \beta_j^2}{2\sigma^2 \nu} t\right) dt \frac{1}{\nu} \\
&= \frac{\Gamma(\frac{\nu+1}{2})}{\nu^{\frac{\nu+1}{2}}} U\left(\frac{\nu+1}{2}, 1, \frac{\xi \beta_j^2}{2\sigma^2 \nu}\right) \\
&\propto U\left(\frac{\nu+1}{2}, 1, \frac{\xi \beta_j^2}{2\sigma^2 \nu}\right), \tag{14}
\end{aligned}$$

where Equation (14) follows from the definition of the confluent hypergeometric function of the second kind: $U(a, b, z) := \frac{1}{\Gamma(a)} \int_0^\infty x^{a-1} (1+x)^{b-a-1} e^{-zx} dx$ for any $a, b, z > 0$. By the asymptotic expansion of the confluent hypergeometric function of the second kind [Abramowitz, 1974, Section 13.1], we obtain

$$\pi(\beta_j | \xi, \sigma^2) \propto U\left(\frac{\nu+1}{2}, 1, \frac{\xi \beta_j^2}{2\sigma^2 \nu}\right) \asymp \begin{cases} -\frac{1}{\Gamma(\frac{1+\nu}{2})} \log\left(\frac{\xi \beta_j^2}{2\sigma^2 \nu}\right) & \asymp -\log(|\beta_j|) \text{ for } |\beta_j| \rightarrow 0 \\ \left(\frac{\xi \beta_j^2}{2\sigma^2 \nu}\right)^{-\frac{1+\nu}{2}} & \asymp |\beta_j|^{-(1+\nu)} \text{ for } |\beta_j| \rightarrow +\infty \end{cases} \tag{15}$$

as required for Equation (4).

Marginal Posterior of β . Let π_ξ denote the prior density on ξ and π_{σ^2} the $\text{InvGamma}(\frac{a_0}{2}, \frac{b_0}{2})$ prior density on σ^2 . Then,

$$\pi(\beta | \xi, \sigma^2, y) \propto \mathcal{N}(y; X\beta, \sigma^2 I_n) \left(\prod_{j=1}^p \pi(\beta_j | \xi, \sigma^2) \right) \propto \mathcal{N}(y; X\beta, \sigma^2 I_n) \prod_{j=1}^p U\left(\frac{1+\nu}{2}, 1, \frac{\xi \beta_j^2}{2\sigma^2 \nu}\right) \tag{16}$$

as required for Equation (5). Equations (15) and (16) directly give

$$\pi(\beta | \xi, \sigma^2, y) \asymp \prod_{j=1}^p U\left(\frac{\nu+1}{2}, 1, \frac{\xi \beta_j^2}{2\sigma^2 \nu}\right) \asymp - \prod_{j=1}^p \log |\beta_j| \text{ for } \|\beta\| \rightarrow 0.$$

Gradient of negative log-density of posterior of β . From Equation (16), we obtain

$$\begin{aligned}
-\frac{\partial}{\partial \beta_j} \left(\log \pi(\beta | \xi, \sigma^2, y) \right) &= -\frac{\partial}{\partial \beta_j} \left(-\frac{1}{2\sigma^2} \|y - X\beta\|_2^2 + \sum_{j=1}^p \log U\left(\frac{1+\nu}{2}, 1, \frac{\xi \beta_j^2}{2\sigma^2 \nu}\right) \right) \\
&= -\left[\frac{1}{\sigma^2} X^T (y - X\beta) \right]_j - \frac{\frac{d}{d\beta_j} U\left(\frac{1+\nu}{2}, 1, \frac{\xi \beta_j^2}{2\sigma^2 \nu}\right)}{U\left(\frac{1+\nu}{2}, 1, \frac{\xi \beta_j^2}{2\sigma^2 \nu}\right)}. \tag{17}
\end{aligned}$$

Recall [Abramowitz, 1974, Section 13.4] for $a, b > 0$,

$$\frac{d}{dz} U(a, b, z) \stackrel{z \geq 0}{\asymp} -a U(a+1, b+1, z), \quad U(a, 2, z) \stackrel{z \rightarrow 0^+}{\asymp} \frac{1}{\Gamma(a)} \frac{1}{z}, \quad U(a, 1, z) \stackrel{z \rightarrow 0^+}{\asymp} -\frac{1}{\Gamma(a)} \log(z).$$

This gives

$$\frac{\frac{d}{d\beta_j} U\left(\frac{1+\nu}{2}, 1, \frac{\xi\beta_j^2}{2\sigma^2\nu}\right)}{U\left(\frac{1+\nu}{2}, 1, \frac{\xi\beta_j^2}{2\sigma^2\nu}\right)} = -\frac{1+\nu}{2} \frac{U\left(\frac{1+\nu}{2} + 1, 1 + 1, \frac{\xi\beta_j^2}{2\sigma^2\nu}\right)}{U\left(\frac{1+\nu}{2}, 1, \frac{\xi\beta_j^2}{2\sigma^2\nu}\right)} \frac{\xi\beta_j}{\sigma^2\nu} \underset{\beta_j \rightarrow 0}{\asymp} \frac{1}{\beta_j \log|\beta_j|}.$$

Therefore by Equation (17), $-\frac{\partial}{\partial\beta_j} \left(\log \pi(\beta|\xi, \sigma^2, y) \right) \underset{\beta_j \rightarrow 0}{\asymp} -\frac{1}{\beta_j \log|\beta_j|}$ as required. \square

Proof of Corollary 2.2. By Proposition 2.1,

$$\pi(\beta|\xi, \sigma^2, y) = \frac{1}{Z_{\xi, \sigma^2, \nu}} \mathcal{N}(y; X\beta, \sigma^2 I_n) \prod_{j=1}^p U\left(\frac{1+\nu}{2}, 1, \frac{\xi\beta_j^2}{2\sigma^2\nu}\right),$$

where $Z_{\xi, \sigma^2, \nu} := \int_{\mathbb{R}^p} \mathcal{N}(y; X\beta, \sigma^2 I_n) \prod_{j=1}^p U\left(\frac{1+\nu}{2}, 1, \frac{\xi\beta_j^2}{2\sigma^2\nu}\right) d\beta$ is the normalizing constant. As $p > n$, there exists some $\beta^\perp \in \mathbb{R}^p$ such that $X\beta^\perp = 0$. For any such fixed such β^\perp and large $\lambda > 0$, we obtain

$$\begin{aligned} \pi(\lambda\beta^\perp|\xi, \sigma^2, y) &= \frac{1}{Z_{\xi, \sigma^2, \nu}} \mathcal{N}(y; 0, \sigma^2 I_n) \prod_{j=1}^p U\left(\frac{1+\nu}{2}, 1, \frac{\xi\lambda^2(\beta_j^\perp)^2}{2\sigma^2\nu}\right) \\ &\propto \prod_{j=1}^p U\left(\frac{1+\nu}{2}, 1, \frac{\xi\lambda^2(\beta_j^\perp)^2}{2\sigma^2\nu}\right) \\ &\asymp \prod_{j=1}^p \left(\frac{\xi\lambda^2(\beta_j^\perp)^2}{2\sigma^2\nu}\right)^{-\frac{1+\nu}{2}} \\ &\asymp \lambda^{-p(1+\nu)}, \end{aligned} \tag{18}$$

where Equation (18) follows from the asymptotic expansion of the confluent hypergeometric function of the second kind [Abramowitz, 1974, Section 13.1]. \square

A.2 Geometric Ergodicity

Initial technical results. We first record some technical results.

Lemma A.1. *(A uniform bound on the full conditional mean of β).* For all $\xi > 0$ and $\eta \in (0, \infty)^p$,

$$\|(X^T X + \xi \text{Diag}(\eta))^{-1} X^T y\|_2 \leq \|y\|_2 \frac{1}{\sigma_{\min > 0}(X)},$$

where $\|\cdot\|_2$ is the L_2 norm and $\sigma_{\min > 0}(X)$ is the smallest non-zero singular value of X .

Proof. Denote $R := \xi \text{Diag}(\eta)$, and choose some $\epsilon > 0$ such that $0 < \epsilon < \xi(\min_{j=1}^p \eta_j)$. Then $\Delta := R - \epsilon I_p$ is a diagonal matrix with positive entries. We obtain

$$\begin{aligned} (X^T X + R)^{-1} X^T y &= (X^T X + \epsilon I_p + \Delta)^{-1} X^T y \\ &= \left((X^T X + \epsilon I_p)^{-1} (X^T X + \epsilon I_p + \Delta) \right)^{-1} \left((X^T X + \epsilon I_p)^{-1} X^T y \right) \\ &= \left(I_p + (X^T X + \epsilon I_p)^{-1} \Delta \right)^{-1} \left((X^T X + \epsilon I_p)^{-1} X^T y \right). \end{aligned} \tag{19}$$

Note that the matrix $(X^T X + \epsilon I_p)^{-1} \Delta$ has only positive eigenvalues, as it is similar to the positive-definite matrix $\Delta^{1/2} (X^T X + \epsilon I_p)^{-1} \Delta^{1/2}$. Therefore, all eigenvalues of $I_p + (X^T X + \epsilon I_p)^{-1} \Delta$ are greater than 1 and $\|(I_p + (X^T X + \epsilon I_p)^{-1} \Delta)^{-1}\|_2 \leq 1$, where $\|\cdot\|_2$ is the L_2 operator norm of a matrix. By submultiplicity of matrix operator norms, Equation (19) gives

$$\begin{aligned} \|(X^T X + R)^{-1} X^T y\|_2 &\leq \|(I_p + (X^T X + \epsilon I_p)^{-1} \Delta)^{-1}\|_2 \|(X^T X + \epsilon I_p)^{-1} X^T y\|_2 \\ &\leq \|(X^T X + \epsilon I_p)^{-1} X^T y\|_2. \end{aligned}$$

We now bound $\|(X^T X + \epsilon I_p)^{-1} X^T y\|_2$ uniformly across all $\epsilon > 0$. Consider the singular value decomposition of X , given by $X = UDV^T$ for U an $n \times n$ orthogonal matrix, V an $p \times p$ orthogonal matrix, and D an $n \times p$ diagonal matrix, such that $D = (\tilde{D}_n \ 0_{n,p-n})$ where $\tilde{D}_n := \text{Diag}(\tilde{D}_{jj})$ is an $n \times n$ diagonal matrix with non-negative entries $(\tilde{D}_{jj})_{j=1}^n$ and $0_{n,p-n}$ is an $n \times (p-n)$ matrix of zeroes. Then,

$$\begin{aligned} \|(X^T X + \epsilon I_p)^{-1} X^T y\|_2 &= \|(VD^T DV^T + \epsilon VV^T)^{-1} VD^T U^T y\|_2 \\ &= \|V(D^T D + \epsilon I_p)^{-1} V^T VD^T U^T y\|_2 \\ &= \|(D^T D + \epsilon I_p)^{-1} D^T U^T y\|_2. \end{aligned} \quad (20)$$

Note that

$$(D^T D + \epsilon I_p)^{-1} D^T = \begin{pmatrix} \tilde{D}_n^2 + \epsilon I_n & 0_{n,p-n} \\ 0_{p-n,n} & \epsilon I_{p-n} \end{pmatrix}^{-1} \begin{pmatrix} \tilde{D}_n \\ 0_{p-n,n} \end{pmatrix} = \begin{pmatrix} (\tilde{D}_n^2 + \epsilon I_n)^{-1} \tilde{D}_n \\ 0_{p-n,n} \end{pmatrix}.$$

Therefore by Equation (20),

$$\begin{aligned} \|(X^T X + \epsilon I_p)^{-1} X^T y\|_2 &= \| \begin{pmatrix} (\tilde{D}_n^2 + \epsilon I_n)^{-1} \tilde{D}_n \\ 0_{p-n,n} \end{pmatrix} U^T y \|_2 \\ &= \|(\tilde{D}_n^2 + \epsilon I_n)^{-1} \tilde{D}_n U^T y\|_2 \\ &= \| \text{Diag} \left(\frac{\tilde{D}_{jj}}{\tilde{D}_{jj}^2 + \epsilon} \right)_{j=1}^n U^T y \|_2 \\ &\leq \| \text{Diag} \left(\frac{\tilde{D}_{jj}}{\tilde{D}_{jj}^2 + \epsilon} \right)_{j=1}^n \|_2 \|U^T y\|_2 \\ &\leq \frac{1}{\min_{j: \tilde{D}_{jj} > 0} \tilde{D}_{jj}} \|U^T y\|_2 \\ &= \left(\frac{1}{\min_{j: \tilde{D}_{jj} > 0} \tilde{D}_{jj}} \right) \|y\|_2 \\ &= \frac{1}{\sigma_{\min > 0}(X)} \|y\|_2 \end{aligned} \quad (21)$$

as required, where Equation (21) follows as $\frac{\tilde{D}_{jj}}{\tilde{D}_{jj}^2 + \epsilon} \leq \frac{1}{\tilde{D}_{jj}} \mathbb{1}\{\tilde{D}_{jj} > 0\}$ for all $j = 1, \dots, n$. \square

Remark A.2. We could tighten the uniform upper bound in Lemma A.1. Note that $\|(X^T X + \epsilon I_p)^{-1} X^T y\|_2$ is a decreasing function of $\epsilon > 0$, and

$$\lim_{\epsilon \rightarrow 0} \|(X^T X + \epsilon I_p)^{-1} X^T y\|_2 = \|X^\dagger y\|_2 \quad (22)$$

for X^\dagger the Moore-Penrose pseudoinverse of matrix X . When $n \geq p$, $X^\dagger = (X^T X)^{-1} X^T$ and we recover the well-known result [Hoerl and Kennard, 1970] that ridge regression produces estimates with smaller norms compared to ordinary least squares. Equation (22) generalizes this insight to the high-dimensional setting.

Lemma A.3. (Moments of the full conditionals of each η_j). For fixed constants $m > 0$ and $\nu > 0$, define a distribution on $(0, \infty)$ with probability density function

$$p(\eta | m) \propto \frac{1}{\eta^{\frac{1-\nu}{2}} (1 + \nu\eta)^{\frac{\nu+1}{2}}} e^{-m\eta}. \quad (23)$$

Then for any $c > \max\{-\frac{\nu+1}{2}, -1\}$ and $\eta \sim p(\cdot | m)$, we have

$$\mathbb{E}[\eta^c | m] = \frac{1}{\nu^c} \frac{\Gamma(\frac{1+\nu}{2} + c)}{\Gamma(\frac{1+\nu}{2})} \frac{U(\frac{1+\nu}{2} + c, 1 + c, \frac{m}{\nu})}{U(\frac{1+\nu}{2}, 1, \frac{m}{\nu})}.$$

Proof. Recall the definition of the confluent hypergeometric function of the second kind $U(a, b, z) := \frac{1}{\Gamma(a)} \int_0^\infty x^{a-1} (1+x)^{b-a-1} e^{-zx} dx$. We obtain

$$\begin{aligned} \int_0^\infty \frac{\eta^c}{\eta^{\frac{1-\nu}{2}} (1+\nu\eta)^{\frac{\nu+1}{2}}} e^{-m\eta} d\eta &= \nu^{-\frac{\nu+1}{2}-c} \int_0^\infty x^{\frac{\nu+1}{2}+c-1} (1+x)^{-\frac{\nu+1}{2}} e^{-\frac{m}{\nu}x} dx \\ &= \nu^{-\frac{\nu+1}{2}-c} \Gamma\left(\frac{\nu+1}{2}+c\right) U\left(\frac{\nu+1}{2}+c, 1+c, \frac{m}{\nu}\right). \end{aligned}$$

Therefore,

$$\begin{aligned} \mathbb{E}[\eta^c | m] &= \frac{\nu^{-\frac{\nu+1}{2}-c} \Gamma\left(\frac{\nu+1}{2}+c\right) U\left(\frac{\nu+1}{2}+c, 1+c, \frac{m}{\nu}\right)}{\nu^{-\frac{\nu+1}{2}} \Gamma\left(\frac{\nu+1}{2}\right) U\left(\frac{\nu+1}{2}, 1, \frac{m}{\nu}\right)} \\ &= \frac{1}{\nu^c} \frac{\Gamma\left(\frac{\nu+1}{2}+c\right) U\left(\frac{\nu+1}{2}+c, 1+c, \frac{m}{\nu}\right)}{\Gamma\left(\frac{\nu+1}{2}\right) U\left(\frac{\nu+1}{2}, 1, \frac{m}{\nu}\right)}. \end{aligned}$$

□

Ratios of confluent hypergeometric function evaluations, such as the ones arising in Lemma A.3, can be upper-bounded using the following result.

Lemma A.4. *Let U denote the confluent hypergeometric function of the second kind, and fix $r > 0$.*

1. *Let $c > 0$. Then for every $\epsilon > 0$, there exists a $K_{\epsilon,c,r}^{(1)} < \infty$ such that*

$$\frac{U(r+c, 1+c, x)}{U(r, 1, x)} < \epsilon x^{-c} + K_{\epsilon,c,r}^{(1)} \quad \text{for all } x > 0.$$

2. *Let $\max\{-1, -r\} < c < 0$. Then there exists some $K_{c,r}^{(2)} < \infty$ such that*

$$\frac{U(r+c, 1+c, x)}{U(r, 1, x)} < x^{-c} + K_{c,r}^{(2)} \quad \text{for all } x > 0.$$

Proof.

Case: $c > 0$. By definition, we have

$$\frac{\Gamma(r+c)U(r+c, 1+c, x)}{\Gamma(r)U(r, 1, x)} = \frac{\int_0^\infty t^{r+c-1} (1+t)^{-r} e^{-xt} dt}{\int_0^\infty t^{r-1} (1+t)^{-r} e^{-xt} dt} = \mathbb{E}[T_x^c] = x^{-c} \mathbb{E}[Y_x^c]$$

where T_x is a random variable with density $p_{T_x}(t) \propto t^{r-1} (1+t)^{-r} e^{-xt}$ on $[0, \infty)$, and $Y_x := xT_x$ is a random variable with density $p_{Y_x}(t) \propto y^{r-1} (x+y)^{-r} e^{-y}$ on $[0, \infty)$.

1. Consider $\mathbb{E}[Y_x^c]$ as $x \rightarrow 0^+$. We obtain

$$\lim_{x \rightarrow 0^+} \mathbb{E}[Y_x^c] = \lim_{x \rightarrow 0^+} \frac{\int_0^\infty y^{c+r-1} (x+y)^{-r} e^{-y} dy}{\int_0^\infty y^{r-1} (x+y)^{-r} e^{-y} dy} = \frac{\Gamma(c)}{\lim_{x \rightarrow 0^+} \int_0^\infty \left(\frac{y}{x+y}\right)^r y^{-1} e^{-y} dy} = 0.$$

2. Consider $\mathbb{E}[T_x^c]$ as a function of x for $x > 0$. From the density of T_x , we note that for all $0 < x_1 < x_2$, T_{x_1} stochastically dominates T_{x_2} , and as $c > 0$, $T_{x_1}^c$ also stochastically dominates $T_{x_2}^c$. Therefore, $\mathbb{E}[T_x^c]$ is a decreasing function of x for $x > 0$.

As $\lim_{x \rightarrow 0^+} \mathbb{E}[Y_x^c] = 0$, for any $\epsilon > 0$, there exists $\delta > 0$ such that $\mathbb{E}[Y_x^c] < \frac{\Gamma(r+c)}{\Gamma(r)} \epsilon$ for all $x \leq \delta$. This gives $x^{-c} \mathbb{E}[Y_x^c] < \frac{\Gamma(r+c)}{\Gamma(r)} \epsilon x^{-c}$ for all $x \leq \delta$. Also for all $x > \delta$, we have $x^{-c} \mathbb{E}[Y_x^c] = \mathbb{E}[T_x^c] \leq \mathbb{E}[T_\delta^c] < \infty$ as $\mathbb{E}[T_x^c]$ is a decreasing function of x for $x > 0$. Overall, we obtain

$$\begin{aligned} \frac{\Gamma(r+c)U(r+c, 1+c, x)}{\Gamma(r)U(r, 1, x)} &= x^{-c} \mathbb{E}[Y_x^c] < \frac{\Gamma(r+c)}{\Gamma(r)} \epsilon x^{-c} + \mathbb{E}[T_\delta^c] \\ &\Rightarrow \frac{U(r+c, 1+c, x)}{U(r, 1, x)} < \epsilon x^{-c} + K_{\epsilon,c,r}^{(1)} \end{aligned}$$

for $K_{\epsilon,c,r}^{(1)} = \frac{\Gamma(r)}{\Gamma(r+c)} \mathbb{E}[T_\delta^c] = \frac{U(r+c, 1+c, \delta)}{U(r, 1, \delta)} < \infty$ as required.

Case: $\max\{-1, -r\} < c < 0$. Note that $U(r+c, 1+c, x)$ and $U(r, 1, x)$ are well-defined as $r, r+c, c+1 > 0$.

1. Consider $\frac{U(r+c, 1+c, x)}{U(r, 1, x)} - x^{-c}$ as $x \rightarrow \infty$. We first recall the asymptotic expansion of the confluent hypergeometric function of the second kind [Abramowitz, 1974, Section 13.5] at infinity,

$$U(a, b, z) = z^{-a} - a(a-b+1)z^{-(a+1)} + \mathcal{O}(z^{-(a+2)}) \quad (24)$$

as $z \rightarrow \infty$ for any $a, b > 0$. For large $x > 0$, this gives

$$\begin{aligned} x^{c+1} \left(\frac{U(r+c, 1+c, x)}{U(r, 1, x)} - x^{-c} \right) &= x^{c+1} \left(\frac{x^r U(r+c, 1+c, x) - x^{r-c} U(r, 1, x)}{x^r U(r, 1, x)} \right) \\ &= x \left(\frac{x^{r+c} U(r+c, 1+c, x) - x^r U(r, 1, x)}{x^r U(r, 1, x)} \right) \\ &= x \left(\frac{\left(1 - \frac{(r+c)r}{x}\right) - \left(1 - \frac{r^2}{x}\right)}{1} + \mathcal{O}(x^{-2}) \right) \\ &= -rc + \mathcal{O}(x^{-1}) \end{aligned} \quad (25)$$

where Equation (25) follows from the asymptotic expansion in Equation (24). As $c+1 > 0$, we obtain

$$\lim_{x \rightarrow \infty} \left(\frac{U(r+c, 1+c, x)}{U(r, 1, x)} - x^{-c} \right) = 0. \quad (26)$$

2. Consider $\frac{U(r+c, 1+c, x)}{U(r, 1, x)} - x^{-c}$ as $x \rightarrow 0^+$. By definition of confluent hypergeometric function of the second kind, we have

$$\lim_{x \rightarrow 0^+} \frac{\Gamma(r+c) U(r+c, 1+c, x)}{\Gamma(r) U(r, 1, x)} = \lim_{x \rightarrow 0^+} \frac{\int_0^\infty t^{r+c-1} (1+t)^{-r} e^{-xt} dt}{\int_0^\infty t^{r-1} (1+t)^{-r} e^{-xt} dt}.$$

Note that as $r+c > 0$ and $c-1 < -1$,

$$\int_0^\infty t^{r+c-1} (1+t)^{-r} dt = \int_0^\infty \left(\frac{t}{1+t}\right)^r t^{c-1} dt \leq \int_0^1 t^{r+c-1} dt + \int_1^\infty t^{c-1} dt = \frac{1}{r+c} - \frac{1}{c} < \infty.$$

Therefore, $\lim_{x \rightarrow 0^+} \int_0^\infty t^{r+c-1} (1+t)^{-r} e^{-xt} dt = \frac{1}{r+c} - \frac{1}{c} < \infty$. However, we have

$$\lim_{x \rightarrow 0^+} \int_0^\infty t^{r-1} (1+t)^{-r} e^{-xt} dt = \lim_{x \rightarrow 0^+} \int_0^\infty \left(\frac{t}{1+t}\right)^r t^{-1} e^{-xt} dt = \infty.$$

Therefore $\lim_{x \rightarrow 0^+} \frac{\Gamma(r+c) U(r+c, 1+c, x)}{\Gamma(r) U(r, 1, x)} = 0$. As $c < 0$, we obtain

$$\lim_{x \rightarrow 0^+} \frac{U(r+c, 1+c, x)}{U(r, 1, x)} - x^{-c} = 0. \quad (27)$$

From Equations (26) and (27), we have $\lim_{x \rightarrow \infty} \frac{U(r+c, 1+c, x)}{U(r, 1, x)} - x^{-c} = 0$ and $\lim_{x \rightarrow 0^+} \frac{U(r+c, 1+c, x)}{U(r, 1, x)} - x^{-c} = 0$.

As $x \mapsto \frac{U(r+c, 1+c, x)}{U(r, 1, x)} - x^{-c}$ is a continuous function on $(0, \infty)$, this implies that $\frac{U(r+c, 1+c, x)}{U(r, 1, x)} - x^{-c}$ is bounded $(0, \infty)$. In particular, there exists some $K_{c,r}^{(2)} < \infty$ such that

$$\frac{U(r+c, 1+c, x)}{U(r, 1, x)} - x^{-c} < K_{c,r}^{(2)}$$

for all $x > 0$ as required. \square

Corollary A.5. (Bound on moments of the full conditionals of each η_j). Consider a random variable η on $(0, \infty)$ with density as in Equation (23) in Lemma A.3 for some $\nu > 0$.

Consider when $c > 0$. There for every $\epsilon > 0$, there exists some $K_{\epsilon,c,\nu}^{(1)} < \infty$ such that

$$\mathbb{E}[\eta^c|m] \leq \epsilon m^{-c} + K_{\epsilon,c,\nu}^{(1)} \quad \text{for all } m > 0.$$

Consider when $\max\{-1, -\frac{1+\nu}{2}\} < c < 0$. Then, there exists some $K_{c,\nu}^{(2)} < \infty$ such that

$$\mathbb{E}[\eta^c|m] \leq \frac{\Gamma(\frac{1+\nu}{2} + c)}{\Gamma(\frac{1+\nu}{2})} m^{-c} + K_{c,\nu}^{(2)} \quad \text{for all } m > 0.$$

Proof. By Lemma A.3, for all $\max\{-1, -\frac{1+\nu}{2}\} < c$,

$$\mathbb{E}[\eta^c|m] = \frac{1}{\nu^c} \frac{\Gamma(\frac{1+\nu}{2} + c)}{\Gamma(\frac{1+\nu}{2})} \frac{U(\frac{1+\nu}{2} + c, 1 + c, \frac{m}{\nu})}{U(\frac{1+\nu}{2}, 1, \frac{m}{\nu})}.$$

Consider when $c > 0$. We apply Lemma A.4 with $r = \frac{1+\nu}{2}$, $x = \frac{m}{\nu}$, and $\tilde{\epsilon} = \epsilon \left(\frac{\Gamma(\frac{1+\nu}{2} + c)}{\Gamma(\frac{1+\nu}{2})} \right)^{-1}$. Then there exists some $\tilde{K}_{\epsilon,c,\nu}^{(1)} < \infty$ such that

$$\mathbb{E}[\eta^c|m] \leq \frac{1}{\nu^c} \frac{\Gamma(\frac{1+\nu}{2} + c)}{\Gamma(\frac{1+\nu}{2})} \left(\tilde{\epsilon} \left(\frac{m}{\nu} \right)^{-c} + \tilde{K}_{\epsilon,c,\nu}^{(1)} \right) = \epsilon m^{-c} + K_{\epsilon,c,\nu}^{(1)}$$

for $K_{\epsilon,c,\nu}^{(1)} = \frac{1}{\nu^c} \frac{\Gamma(\frac{1+\nu}{2} + c)}{\Gamma(\frac{1+\nu}{2})} \tilde{K}_{\epsilon,c,\nu}^{(1)} < \infty$.

Consider when $\max\{-1, -\frac{1+\nu}{2}\} < c < 0$. By Lemma A.4 with $r = \frac{1+\nu}{2}$ and $x = \frac{m}{\nu}$, there exists some $\tilde{K}_{c,\nu}^{(2)} < \infty$ such that

$$\mathbb{E}[\eta^c|m] \leq \frac{1}{\nu^c} \frac{\Gamma(\frac{1+\nu}{2} + c)}{\Gamma(\frac{1+\nu}{2})} \left(\left(\frac{m}{\nu} \right)^{-c} + \tilde{K}_{c,\nu}^{(2)} \right) = \frac{\Gamma(\frac{1+\nu}{2} + c)}{\Gamma(\frac{1+\nu}{2})} m^{-c} + K_{c,\nu}^{(2)}$$

for $K_{c,\nu}^{(2)} = \frac{1}{\nu^c} \frac{\Gamma(\frac{1+\nu}{2} + c)}{\Gamma(\frac{1+\nu}{2})} \tilde{K}_{c,\nu}^{(2)} < \infty$. □

Lemma A.6. Let $X \sim \mathcal{N}(\mu, \sigma^2)$ on \mathbb{R} . Then, for $c \in (0, 1)$,

$$\mathbb{E}[|X|^{-c}] \leq \frac{1}{\sigma^c 2^{c/2}} \frac{\Gamma(\frac{1-c}{2})}{\sqrt{\pi}}$$

Proof. We follow the proof in Johndrow et al. [2020], which is included here for completeness. Recall the inverse moments of the univariate Normal distribution,

$$\mathbb{E}[|X|^{-c}] = \frac{1}{\sigma^c 2^{c/2}} \frac{\Gamma(\frac{1-c}{2})}{\sqrt{\pi}} \exp\left(-\frac{\mu^2}{2\sigma^2}\right) M\left(\frac{1-c}{2}, \frac{1}{2}, \frac{\mu^2}{2\sigma^2}\right)$$

where $M(a, b, z) := {}_1F_1(a; b; z)$ is the confluent hypergeometric function of the first kind. For $a < b$, we know $M(a, b, z) = \frac{\Gamma(b)}{\Gamma(a)\Gamma(b-a)} \int_0^1 e^{zt} t^{a-1} (1-t)^{b-a-1} dt$. For $a = \frac{1-c}{2} < b = \frac{1}{2}$ and $z = \frac{\mu^2}{2\sigma^2}$, this gives

$$\begin{aligned} \exp(-z) M(a, b, z) &= \frac{\Gamma(b)}{\Gamma(a)\Gamma(b-a)} \int_0^1 e^{-z(1-t)} t^{a-1} (1-t)^{b-a-1} dt \\ &= \frac{\Gamma(b)}{\Gamma(a)\Gamma(b-a)} \int_0^1 e^{-zt} (1-t)^{a-1} t^{b-a-1} dt. \end{aligned}$$

Therefore, $\exp(-z) M(a, b, z)$ is decreasing for $z \geq 0$ and $\exp(-z) M(a, b, z) \leq \exp(-0) M(a, b, 0) = 1$ for all $z \geq 0$. This gives

$$\mathbb{E}[|X|^{-c}] = \frac{1}{\sigma^c 2^{c/2}} \frac{\Gamma(\frac{1-c}{2})}{\sqrt{\pi}} \exp\left(-\frac{\mu^2}{2\sigma^2}\right) M\left(\frac{1-c}{2}, \frac{1}{2}, \frac{\mu^2}{2\sigma^2}\right) \leq \frac{1}{\sigma^c 2^{c/2}} \frac{\Gamma(\frac{1-c}{2})}{\sqrt{\pi}}.$$

□

Lemma A.7. (A uniform bound on the full conditional mean of $1/\sigma^2$). Consider the full conditional distribution of σ^2 given η, ξ in Algorithm 1. Given $\eta \in \mathbb{R}_{>0}^p, \xi > 0$, we have

$$\sigma^2 | \xi, \eta \sim \text{InvGamma}\left(\frac{a_0 + n}{2}, \frac{y^T M_{\xi, \eta}^{-1} y + b_0}{2}\right),$$

where $M_{\xi, \eta} = I_n + \xi^{-1} X \text{Diag}(\eta^{-1}) X^T$. Then

$$\mathbb{E}\left[\frac{1}{\sigma^2} | \xi, \eta\right] = \frac{a_0 + n}{y^T M_{\xi, \eta}^{-1} y + b_0} < \frac{a_0 + n}{b_0} < \infty. \quad (28)$$

Proof. Recall that the mean of a $\text{Gamma}(a, b)$ distribution (under shape and rate parameterization) is a/b . Equation (28) now directly follows as $M_{\xi, \eta}^{-1}$ is positive semi-definite. \square

Drift and Minorization conditions.

Proof of Proposition 2.3. For ease of notation, denote $\Sigma_{t+1} := X^T X + \xi_{t+1} \text{Diag}(\eta_{t+1})$ and let e_j be the j^{th} unit vector of the standard basis on \mathbb{R}^p . We first consider $\sum_{j=1}^p m_j^d$. Note that

$$\begin{aligned} \mathbb{E}\left[\sum_{j=1}^p m_{j, t+1}^d | \eta_{t+1}, \xi_{t+1}, \sigma_{t+1}^2\right] &= \left(\frac{\xi_{t+1}}{2\sigma_{t+1}^2}\right)^d \sum_{j=1}^p \mathbb{E}\left[|\beta_{j, t+1}|^{2d} | \eta_{t+1}, \xi_{t+1}, \sigma_{t+1}^2\right] \\ &\leq \left(\frac{\xi_{t+1}}{2\sigma_{t+1}^2}\right)^d \sum_{j=1}^p \mathbb{E}\left[\beta_{j, t+1}^2 | \eta_{t+1}, \xi_{t+1}, \sigma_{t+1}^2\right]^d \end{aligned} \quad (29)$$

$$\begin{aligned} &= \left(\frac{\xi_{t+1}}{2\sigma_{t+1}^2}\right)^d \sum_{j=1}^p \left(\left(e_j^T \Sigma_{t+1}^{-1} X^T y\right)^2 + \sigma_{t+1}^2 (e_j^T \Sigma_{t+1}^{-1} e_j)\right)^d \\ &\leq \left(\frac{\xi_{t+1}}{2\sigma_{t+1}^2}\right)^d \sum_{j=1}^p \left(|e_j^T \Sigma_{t+1}^{-1} X^T y|^{2d} + \sigma_{t+1}^{2d} (e_j^T \Sigma_{t+1}^{-1} e_j)^d\right) \end{aligned} \quad (30)$$

$$\begin{aligned} &\leq \left(\frac{\xi_{t+1}}{2\sigma_{t+1}^2}\right)^d \left(\sum_{j=1}^p (|e_j^T \Sigma_{t+1}^{-1} X^T y|^{2d})^{1/d}\right)^d p^{1-d} \\ &\quad + \sigma_{t+1}^{2d} \left(\frac{\xi_{t+1}}{2\sigma_{t+1}^2}\right)^d \sum_{j=1}^p (e_j^T (\xi_{t+1} \text{Diag}(\eta_{t+1}))^{-1} e_j)^d \end{aligned} \quad (31)$$

$$\begin{aligned} &= \left(\frac{\xi_{t+1}}{2\sigma_{t+1}^2}\right)^d \left(\|\Sigma_{t+1}^{-1} X^T y\|_2^2\right)^d p^{1-d} + \frac{1}{2^d} \sum_{j=1}^p \frac{1}{\eta_{j, t+1}^d} \\ &\leq \left(\frac{\xi_{t+1}}{2\sigma_{t+1}^2}\right)^d \left(\frac{\|y\|_2^2}{\sigma_{\min > 0}(X)^2}\right)^d p^{1-d} + \frac{1}{2^d} \sum_{j=1}^p \frac{1}{\eta_{j, t+1}^d}, \end{aligned} \quad (32)$$

where Equation (29) follows from Jensen's inequality, Equation (30) follows as $(x+y)^d \leq x^d + y^d$ for $x, y \geq 0$ and $d \in (0, 1)$, Equation (31) follows from Hölder's inequality and from $e_j^T \Sigma_{t+1}^{-1} e_j \leq e_j^T (\xi_{t+1} \text{Diag}(\eta_{t+1}))^{-1} e_j$ as $X^T X$ is positive-definite matrix, and Equation (32) follows from Lemma A.1.

As the prior $\pi_\xi(\cdot)$ on ξ has compact support, we have $b \leq \xi_{t+1} \leq B$ for all $t \geq 0$ for some $0 < b \leq B < \infty$. This upper bound on ξ_{t+1} , Lemma A.7 and Jensen's inequality gives

$$\mathbb{E}\left[\left(\frac{\xi_{t+1}}{2\sigma_{t+1}^2}\right)^d | \eta_{t+1}\right] \leq \frac{B^d}{2^d} \mathbb{E}\left[\left(\frac{1}{\sigma_{t+1}^2}\right) | \eta_{t+1}\right]^d \leq \frac{B^d}{2^d} \left(\frac{a_0 + n}{b_0}\right)^d = \left(\frac{B(a_0 + n)}{2b_0}\right)^d. \quad (33)$$

Therefore, by Equations (32) and (33), we obtain

$$\mathbb{E}\left[\sum_{j=1}^p m_{j, t+1}^d | \eta_{t+1}\right] = \mathbb{E}\left[\mathbb{E}\left[\sum_{j=1}^p m_{j, t+1}^d | \eta_{t+1}, \xi_{t+1}, \sigma_{t+1}^2\right] | \eta_{t+1}\right] \leq \frac{1}{2^d} \sum_{j=1}^p \frac{1}{\eta_{j, t+1}^d} + K_1 \quad (34)$$

for $K_1 := \left(\frac{B(a_0+n)}{2b_0} \right)^d \left(\frac{\|y\|_2^2}{\sigma_{min>0}(X)^2} \right)^d p^{1-d} < \infty$. By Equation (34) and Corollary A.5, we obtain

$$\begin{aligned}
\mathbb{E} \left[\sum_{j=1}^p m_{j,t+1}^d | \beta_t, \xi_t, \sigma_t^2 \right] &= \mathbb{E} \left[\mathbb{E} \left[\sum_{j=1}^p m_{j,t+1}^d | \eta_{t+1} \right] | \beta_t, \xi_t, \sigma_t^2 \right] \\
&\leq \frac{1}{2^d} \sum_{j=1}^p \mathbb{E} \left[\eta_{j,t+1}^{-d} | \beta_t, \xi_t, \sigma_t^2 \right] + K_1 \\
&\leq \frac{1}{2^d} \left(\sum_{j=1}^p \frac{\Gamma(\frac{1+\nu}{2} - d)}{\Gamma(\frac{1+\nu}{2})} m_{j,t}^d + K_{d,\nu}^{(2)} \right) + K_1 \\
&\leq \frac{1}{2^d} \frac{\Gamma(\frac{1+\nu}{2} - d)}{\Gamma(\frac{1+\nu}{2})} \sum_{j=1}^p m_{j,t}^d + K_2
\end{aligned} \tag{35}$$

for $K_2 := \frac{p}{2^d} K_{d,\nu}^{(2)} + K_1 < \infty$. Note that for every $\nu \geq 1$, there exists $d \in (0, 1)$ such that $\frac{1}{2^d} \frac{\Gamma(\frac{\nu+1}{2} - d)}{\Gamma(\frac{\nu+1}{2})} < 1$.

We can verify this by considering the function $f(d) := \frac{1}{2^d} \frac{\Gamma(\frac{\nu+1}{2} - d)}{\Gamma(\frac{\nu+1}{2})}$. It suffices to note that $f(0) = 1$ and $f'(0) = -\psi(\frac{\nu+1}{2}) - \log(2) < 0$ for $\nu \geq 1$, where $\psi(x) := \frac{\Gamma'(x)}{\Gamma(x)}$ is the Digamma function.

We now consider $\sum_{j=1}^p m_j^{-c}$ for $c \in (0, 1/2)$. We obtain

$$\begin{aligned}
\mathbb{E} \left[\sum_{j=1}^p m_{j,t+1}^{-c} | \sigma_{t+1}^2, \xi_{t+1}, \eta_{t+1} \right] &= \left(\frac{\xi_{t+1}}{2\sigma_{t+1}^2} \right)^{-c} \sum_{j=1}^p \mathbb{E} \left[|\beta_{j,t+1}|^{-2c} | \sigma_{t+1}^2, \xi_{t+1}, \eta_{t+1} \right] \\
&\leq \left(\frac{\xi_{t+1}}{2\sigma_{t+1}^2} \right)^{-c} \frac{1}{2^c} \frac{\Gamma(\frac{1-2c}{2})}{\sqrt{\pi}} \sum_{j=1}^p (\sigma_{t+1}^2 e_j^T \Sigma_{t+1}^{-1} e_j)^{-c}
\end{aligned} \tag{36}$$

$$\leq \left(\frac{\xi_{t+1}}{2\sigma_{t+1}^2} \right)^{-c} \frac{1}{2^c} \frac{\Gamma(\frac{1-2c}{2})}{\sqrt{\pi}} \sum_{j=1}^p (\sigma_{t+1}^2 e_j^T (\|X\|_2^2 I_p + \xi_{t+1} Diag(\eta_{t+1}))^{-1} e_j)^{-c} \tag{37}$$

$$\begin{aligned}
&= \left(\frac{\xi_{t+1}}{2\sigma_{t+1}^2} \right)^{-c} \frac{1}{2^c} \frac{\Gamma(\frac{1-2c}{2})}{\sqrt{\pi}} \sum_{j=1}^p \frac{(\|X\|_2^2 + \xi_{t+1} \eta_{j,t+1})^c}{\sigma_{t+1}^{2c}} \\
&\leq \frac{\Gamma(\frac{1}{2} - c)}{\sqrt{\pi}} \sum_{j=1}^p \left(\left(\frac{\|X\|_2^2}{\xi_{t+1}} \right)^c + \eta_{j,t+1}^c \right)
\end{aligned} \tag{38}$$

$$\leq \frac{\Gamma(\frac{1}{2} - c)}{\sqrt{\pi}} \sum_{j=1}^p \eta_{j,t+1}^c + p \frac{\Gamma(\frac{1}{2} - c)}{\sqrt{\pi}} \left(\frac{\|X\|_2^2}{b} \right)^c \tag{39}$$

for some $b > 0$. Here Equation (36) follows from Lemma A.6, Equation (37) follows as $e_j^T (\|X\|_2^2 I_p + \xi_t Diag(\eta_t))^{-1} e_j \leq e_j^T \Sigma_{t+1}^{-1} e_j$ for $\|\cdot\|_2$ the L_2 operator norm of a matrix, Equation (38) follows as $(x+y)^c \leq x^c + y^c$ for all $x, y > 0$ and $0 < c < 1/2$, and Equation (39) follows as the prior on ξ has compact support, so $\xi_{t+1} \geq b$ for some $b > 0$. Therefore, by Equation (39),

$$\mathbb{E} \left[\sum_{j=1}^p m_{j,t+1}^{-c} | \eta_{t+1} \right] = \mathbb{E} \left[\mathbb{E} \left[\sum_{j=1}^p m_{j,t+1}^{-c} | \sigma_{t+1}^2, \xi_{t+1}, \eta_{t+1} \right] | \eta_{t+1} \right] \leq \frac{\Gamma(\frac{1}{2} - c)}{\sqrt{\pi}} \sum_{j=1}^p \eta_{j,t+1}^c + K_3. \tag{40}$$

for $K_3 := p \frac{\Gamma(\frac{1}{2} - c)}{\sqrt{\pi}} \left(\frac{\|X\|_2^2}{b} \right)^c < \infty$. By Equation (40) and Corollary A.5 with $r = \frac{1+\nu}{2}$ and any $\epsilon < \frac{\sqrt{\pi}}{\Gamma(\frac{1}{2} - c)}$,

there exists $K_{\epsilon,c,\nu}^{(1)} < \infty$ such that

$$\begin{aligned}
\mathbb{E} \left[\sum_{j=1}^p m_{j,t+1}^{-c} | \sigma_t^2, \xi_t, \beta_t \right] &= \mathbb{E} \left[\mathbb{E} \left[\sum_{j=1}^p m_{j,t+1}^{-c} | \eta_{t+1} \right] | \sigma_t^2, \xi_t, \beta_t \right] \\
&\leq \frac{\Gamma(\frac{1}{2} - c)}{\sqrt{\pi}} \sum_{j=1}^p \mathbb{E} \left[\eta_{j,t+1}^c | \sigma_t^2, \xi_t, \beta_t \right] + K_3 \\
&\leq \frac{\Gamma(\frac{1}{2} - c)}{\sqrt{\pi}} \sum_{j=1}^p \left(\epsilon m_{j,t}^{-c} + K_{\epsilon,c,\nu}^{(1)} \right) + K_3 \\
&= \left(\frac{\Gamma(\frac{1}{2} - c)}{\sqrt{\pi}} \epsilon \right) \sum_{j=1}^p m_{j,t}^{-c} + K_4,
\end{aligned} \tag{41}$$

where $\frac{\Gamma(\frac{1}{2} - c)}{\sqrt{\pi}} \epsilon < 1$ and $K_4 = p \frac{\Gamma(\frac{1}{2} - c)}{\sqrt{\pi}} K_{\epsilon,c,\nu}^{(1)} + K_3$.

We can now combine Equations (35) and (41) together. Then, for some fixed $d \in (0, 1)$ such that $\frac{1}{2^d} \frac{\Gamma(\frac{\nu+1}{2} - d)}{\Gamma(\frac{\nu+1}{2})} < 1$ and any $c \in (0, 1/2)$, we obtain

$$\mathbb{E} \left[\sum_{j=1}^p m_{j,t+1}^{-c} + m_{j,t+1}^d | m_t \right] \leq \gamma_{drift} \left(\sum_{j=1}^p m_{j,t}^{-c} + m_{j,t}^d \right) + K_{drift}$$

for some

$$\begin{aligned}
0 < \gamma_{drift} &:= \max \left\{ \frac{\Gamma(\frac{1}{2} - c)}{\sqrt{\pi}} \epsilon, \frac{1}{2^d} \frac{\Gamma(\frac{\nu+1}{2} - d)}{\Gamma(\frac{\nu+1}{2})} \right\} < 1 \\
0 < K_{drift} &:= K_2 + K_4 < \infty.
\end{aligned}$$

Therefore, for any such $d \in (0, 1)$ and $c \in (0, 1/2)$,

$$V(\beta) = \sum_{j=1}^p m_j^{-c} + m_j^d$$

for $m_j = \frac{\xi \beta_j^2}{2\sigma^2}$ is a Lyapunov function. □

Proof of Proposition 2.4. Take $C^{(i)} = (\beta^{(i)}, \xi^{(i)}, (\sigma^{(i)})^2) \in S(R)$. Note that

$$\begin{aligned}
d_{TV} &\left(\mathcal{P}(C^{(1)}, \cdot), \mathcal{P}(C^{(2)}, \cdot) \right) \\
&= \frac{1}{2} \int p(\beta^* | (\sigma*)^2, \eta^*, \xi^*) p((\sigma*)^2 | \eta^*, \xi^*) p(\xi^* | \eta^*) \left| p(\eta^* | C^{(1)}) - p(\eta^* | C^{(2)}) \right| d\beta^* d((\sigma*)^2) d\xi^* d\eta^* \\
&= \frac{1}{2} \int \left| p(\eta^* | C^{(1)}) - p(\eta^* | C^{(2)}) \right| d\eta^* \\
&= 1 - \int \min \{ p(\eta^* | C^{(1)}), p(\eta^* | C^{(2)}) \} d\eta^* \\
&= 1 - \int \min \left\{ \prod_{j=1}^p p(\eta_j^* | m_j^{(1)}), \prod_{j=1}^p p(\eta_j^* | m_j^{(2)}) \right\} d\eta^* \text{ for } m_j^{(i)} = \frac{\xi^{(i)} (\beta^{(i)})^2}{2 (\sigma^{(i)})^2} \\
&\leq 1 - \int \prod_{j=1}^p \min \left\{ p(\eta_j^* | m_j^{(1)}), p(\eta_j^* | m_j^{(2)}) \right\} d\eta_j^* \\
&= 1 - \prod_{j=1}^p \left(\int \min \left\{ p(\eta_j^* | m_j^{(1)}), p(\eta_j^* | m_j^{(2)}) \right\} d\eta_j^* \right) \\
&= 1 - \prod_{j=1}^p \left(\int \frac{1}{(\eta_j^*)^{\frac{1-\nu}{2}} (1 + \nu \eta_j^*)^{\frac{\nu+1}{2}}} \min \left\{ \frac{e^{-m_j^{(1)} \eta_j}}{U(\frac{1+\nu}{2}, 1, \frac{m_j^{(1)}}{\nu})}, \frac{e^{-m_j^{(2)} \eta_j}}{U(\frac{1+\nu}{2}, 1, \frac{m_j^{(2)}}{\nu})} \right\} d\eta_j^* \right).
\end{aligned}$$

Consider when $R > 1$. As $C^{(1)}, C^{(2)} \in S(R)$, $m_j^{(i)} \in (R^{-1/c}, R^{1/d})$ for all $i = 1, 2$ and $j = 1, \dots, p$. Note also that $x \mapsto U\left(\frac{1+\nu}{2}, 1, x\right)$ is a decreasing function for $x > 0$. This gives, $\frac{e^{-m_j^{(i)} \eta_j}}{U\left(\frac{1+\nu}{2}, 1, \frac{m_j^{(i)}}{\nu}\right)} \geq \frac{e^{-R^{1/d} \eta_j}}{U\left(\frac{1+\nu}{2}, 1, \frac{R^{-1/c}}{\nu}\right)}$ for $i = 1, 2$ and $j = 1, \dots, p$. Therefore,

$$\begin{aligned} d_{TV}\left(\mathcal{P}(\beta^{(1)}, \cdot), \mathcal{P}(\beta^{(2)}, \cdot)\right) &\leq 1 - \prod_{j=1}^p \left(\int \frac{1}{(\eta_j^*)^{\frac{1-\nu}{2}} (1 + \nu \eta_j^*)^{\frac{\nu+1}{2}}} \min \left\{ \frac{e^{-m_j^{(1)} \eta_j}}{U\left(\frac{1+\nu}{2}, 1, \frac{m_j^{(1)}}{\nu}\right)}, \frac{e^{-m_j^{(2)} \eta_j}}{U\left(\frac{1+\nu}{2}, 1, \frac{m_j^{(2)}}{\nu}\right)} \right\} d\eta_j^* \right) \\ &\leq 1 - \prod_{j=1}^p \left(\int \frac{1}{(\eta_j^*)^{\frac{1-\nu}{2}} (1 + \nu \eta_j^*)^{\frac{\nu+1}{2}}} \frac{e^{-R^{1/d} \eta_j}}{U\left(\frac{1+\nu}{2}, 1, \frac{R^{-1/c}}{\nu}\right)} d\eta_j^* \right) \\ &= 1 - \left(\frac{U\left(\frac{1+\nu}{2}, 1, \frac{R^{1/d}}{\nu}\right)}{U\left(\frac{1+\nu}{2}, 1, \frac{R^{-1/c}}{\nu}\right)} \right)^p \\ &= 1 - \epsilon \end{aligned}$$

$$\text{for } \epsilon = \left(\frac{U\left(\frac{1+\nu}{2}, 1, \frac{R^{1/d}}{\nu}\right)}{U\left(\frac{1+\nu}{2}, 1, \frac{R^{-1/c}}{\nu}\right)} \right)^p \in (0, 1) \text{ as } R > 1. \quad \square$$

B Calculating metric d

We present details of estimating the metric d defined in Equation (10). Let $m_{j,t}^{(i)} = \frac{\xi_t^{(i)} (\beta_{j,t}^{(i)})^2}{2(\sigma_t^{(i)})^2}$ for chains $i = 1, 2$. As the coupling in Algorithm 4 is independent component-wise, we have

$$\begin{aligned} d(C_t^{(1)}, C_t^{(2)}) &= 1 - \mathbb{P}_{\text{Algo(4)}}\left(\eta_{t+1}^{(1)} = \eta_{t+1}^{(2)} | C_t^{(1)}, C_t^{(2)}\right) \\ &= 1 - \prod_{j=1}^p \mathbb{P}_{\text{Algo(4)}}\left(\eta_{j,t+1}^{(1)} = \eta_{j,t+1}^{(2)} | \eta_{j,t}^{(1)}, \eta_{j,t}^{(2)}, m_{j,t}^{(1)}, m_{j,t}^{(2)}\right). \end{aligned}$$

B.1 An integration based approximation

We consider the approximation

$$\mathbb{P}_{\text{Algo(4)}}\left(\eta_{j,t+1}^{(1)} \neq \eta_{j,t+1}^{(2)} | \eta_{j,t}^{(1)}, \eta_{j,t}^{(2)}, m_{j,t}^{(1)}, m_{j,t}^{(2)}\right) \approx d_{TV}(M_{j,t}^{(1)}, M_{j,t}^{(2)}),$$

where $M_{j,t}^{(i)}$ for chains $i = 1, 2$ correspond to target distributions of the marginal slice samplers in Algorithm 4. This corresponds to approximating the probability of not meeting under Algorithm 4 with the total variation distance (i.e. probability of not meeting under a maximal coupling) between the marginal target distributions $M_{j,t}^{(1)}, M_{j,t}^{(2)}$ of the slice samplers. We can evaluate $d_{TV}(M_{j,t}^{(1)}, M_{j,t}^{(2)})$ analytically using Proposition B.1. This motivates the approximation

$$\tilde{d}(C_t^{(1)}, C_t^{(2)}) := 1 - \prod_{j=1}^p \left(1 - d_{TV}(M_{j,t}^{(1)}, M_{j,t}^{(2)}) \right)$$

for $d(C_t^{(1)}, C_t^{(2)})$.

Proposition B.1. For $i = 1, 2$, consider distribution $M^{(i)}$ on $[0, \infty)$ with density

$$p(\eta_j | m^{(i)}) \propto \frac{1}{\eta_j^{\frac{1-\nu}{2}} (1 + \nu \eta_j)^{\frac{\nu+1}{2}}} e^{-m^{(i)} \eta_j},$$

such that $M^{(i)}$ is parameterized by the fixed constant $m^{(i)} > 0$. Then, $d_{TV}(M^{(1)}, M^{(2)}) = 0$ when $m^{(1)} = m^{(2)}$. When $m^{(1)} \neq m^{(2)}$,

$$d_{TV}(M^{(1)}, M^{(2)}) = \left| \frac{U_{\frac{1+\nu}{2}, 1, \frac{m^{(1)}}{\nu}}(\nu K)}{U(\frac{1+\nu}{2}, 1, \frac{m^{(1)}}{\nu})} - \frac{U_{\frac{1+\nu}{2}, 1, \frac{m^{(2)}}{\nu}}(\nu K)}{U(\frac{1+\nu}{2}, 1, \frac{m^{(2)}}{\nu})} \right|, \quad (42)$$

where $U_{a,b,z}(t) := \frac{1}{\Gamma(a)} \int_0^t x^{a-1} (1+x)^{b-a-1} e^{-zx} dx$ is defined as the lower incomplete confluent hypergeometric function of the second kind, such that $U_{a,b,z}(\infty) = U(a, b, z)$ gives the confluent hypergeometric function of the second kind, and

$$K := \frac{\log U(\frac{1+\nu}{2}, 1, \frac{m^{(1)}}{\nu}) - \log U(\frac{1+\nu}{2}, 1, \frac{m^{(2)}}{\nu})}{m^{(2)} - m^{(1)}}.$$

Proof. For chains $i = 1, 2$, we have

$$p(\eta_j | m^{(i)}) = \frac{1}{\eta_j^{\frac{1-\nu}{2}} (1 + \nu \eta_j)^{\frac{\nu+1}{2}}} e^{-m^{(i)} \eta_j} \frac{1}{Z^{(i)}},$$

where

$$Z^{(i)} = \int_0^\infty \frac{1}{\eta_j^{\frac{1-\nu}{2}} (1 + \nu \eta_j)^{\frac{\nu+1}{2}}} e^{-m^{(i)} \eta_j} d\eta_j = \nu^{-\frac{\nu+1}{2}} \Gamma\left(\frac{\nu+1}{2}\right) U\left(\frac{\nu+1}{2}, 1, \frac{m^{(i)}}{\nu}\right).$$

Case $m^{(1)} = m^{(2)}$. $d_{TV}(M^{(1)}, M^{(2)}) = 0$ is immediate.

Case $m^{(1)} < m^{(2)}$. Note that

$$\begin{aligned} p(\eta_j | m^{(1)}) \leq p(\eta_j | m^{(2)}) &\Leftrightarrow \exp((m^{(2)} - m^{(1)})\eta_j) \leq \frac{Z^{(1)}}{Z^{(2)}} \\ &\Leftrightarrow \eta \leq \frac{\log(U(\frac{1+\nu}{2}, 1, \frac{m^{(1)}}{\nu})) - \log(U(\frac{1+\nu}{2}, 1, \frac{m^{(2)}}{\nu}))}{m^{(2)} - m^{(1)}} =: K. \end{aligned}$$

Therefore,

$$\begin{aligned} 1 - d_{TV}(M^{(1)}, M^{(2)}) &= \int_0^\infty \min(p(\eta_j | m^{(1)}), p(\eta_j | m^{(2)})) d\eta_j \\ &= \int_0^K p(\eta_j | m^{(1)}) d\eta_j + \int_K^\infty p(\eta_j | m^{(2)}) d\eta_j \\ &= \frac{1}{Z^{(1)}} \int_0^K \frac{1}{\eta_j^{\frac{1-\nu}{2}} (1 + \nu \eta_j)^{\frac{\nu+1}{2}}} e^{-m^{(1)} \eta_j} d\eta_j \\ &\quad + \frac{1}{Z^{(2)}} \int_K^\infty \frac{1}{\eta_j^{\frac{1-\nu}{2}} (1 + \nu \eta_j)^{\frac{\nu+1}{2}}} e^{-m^{(2)} \eta_j} d\eta_j \\ &= \frac{U_{\frac{1+\nu}{2}, 1, \frac{m^{(1)}}{\nu}}(\nu K)}{U(\frac{1+\nu}{2}, 1, \frac{m^{(1)}}{\nu})} + 1 - \frac{U_{\frac{1+\nu}{2}, 1, \frac{m^{(2)}}{\nu}}(\nu K)}{U(\frac{1+\nu}{2}, 1, \frac{m^{(2)}}{\nu})} \\ &= 1 - \left| \frac{U_{\frac{1+\nu}{2}, 1, \frac{m^{(2)}}{\nu}}(\nu K)}{U(\frac{1+\nu}{2}, 1, \frac{m^{(2)}}{\nu})} - \frac{U_{\frac{1+\nu}{2}, 1, \frac{m^{(1)}}{\nu}}(\nu K)}{U(\frac{1+\nu}{2}, 1, \frac{m^{(1)}}{\nu})} \right|. \end{aligned}$$

Equation (42) directly follows.

Case $m^{(1)} > m^{(2)}$. Follows from the $m^{(1)} < m^{(2)}$ case by symmetry. \square

B.2 A Rao-Blackwellized estimator

We have

$$\begin{aligned} \mathbb{P}_{\text{Algo(4)}}\left(\eta_{j,t+1}^{(1)} = \eta_{j,t+1}^{(2)} \mid \eta_{j,t}^{(1)}, \eta_{j,t}^{(2)}, m_{j,t}^{(1)}, m_{j,t}^{(2)}\right) \\ = \mathbb{E}\left[\mathbb{P}_{\max}\left(\eta_{j,t+1}^{(1)} = \eta_{j,t+1}^{(2)} \mid U_{j,*}^{(1)}, U_{j,*}^{(2)}, m_{j,t}^{(1)}, m_{j,t}^{(2)}\right) \mid \eta_{j,t}^{(1)}, \eta_{j,t}^{(2)}, m_{j,t}^{(1)}, m_{j,t}^{(2)}\right], \end{aligned}$$

where $m_{j,t}^{(i)} = \frac{\xi_t^{(i)}(\beta_{j,t}^{(i)})^2}{2(\sigma_t^{(i)})^2}$ for $i = 1, 2$, $(U_{j,*}^{(1)}, U_{j,*}^{(2)})$ are sampled using common random numbers as in Algorithm 4, and \mathbb{P}_{\max} corresponds to the maximal coupling probability. We can analytically evaluate this maximal coupling probability, which motivates a Rao-Blackwellized estimator.

This motivates the estimate from Equation (13),

$$\widehat{d}_R^{(2)}(C_t^{(1)}, C_t^{(2)}) := 1 - \prod_{j=1}^p \left(\frac{1}{R} \sum_{r=1}^R \mathbb{P}_{\max}\left(\eta_{j,t+1}^{(1)} = \eta_{j,t+1}^{(2)} \mid U_{j,r}^{(1)}, U_{j,r}^{(2)}, m_{j,t}^{(1)}, m_{j,t}^{(2)}\right) \right),$$

where R is the number of samples. For each $r = 1, \dots, R$, $(U_{j,r}^{(1)}, U_{j,r}^{(2)})$ is sampled independently as in Algorithm 4 and maximal coupling probability $\mathbb{P}_{\max}\left(\eta_{j,t+1}^{(1)} = \eta_{j,t+1}^{(2)} \mid U_{j,r}^{(1)}, U_{j,r}^{(2)}, m_{j,t}^{(1)}, m_{j,t}^{(2)}\right)$ is calculated analytically using Proposition B.2.

Proposition B.2. For chains $i = 1, 2$, suppose $\eta_j^{(i)} \mid U_{j,*}^{(i)}, m_j^{(i)} \sim P_j^{(i)}$, where each marginal distribution $P_j^{(i)}$ corresponds to distribution P_j of the slice sampler of Algorithm 2. Then,

$$\begin{aligned} \mathbb{P}_{\max}\left(\eta_j^{(1)} = \eta_j^{(2)} \mid U_{j,*}^{(1)}, U_{j,*}^{(2)}, m_j^{(1)}, m_j^{(2)}\right) \\ = \begin{cases} \frac{\gamma_s(m_j^{(1)} \tilde{K}_j)}{\gamma_s(m_j^{(1)} T_{j,*}^{(1)})} + \frac{\gamma_s(m_j^{(2)} (T_{j,*}^{(1)} \wedge T_{j,*}^{(2)})) - \gamma_s(m_j^{(2)} \tilde{K}_j)}{\gamma_s(m_j^{(2)} T_{j,*}^{(2)})} & \text{for } m_j^{(1)} < m_j^{(2)} \\ \frac{\gamma_s(m_j^{(1)} (T_{j,*}^{(1)} \wedge T_{j,*}^{(2)}))}{\gamma_s(m_j^{(1)} (T_{j,*}^{(1)} \vee T_{j,*}^{(2)}))} & \text{for } m_j^{(1)} = m_j^{(2)} \\ \frac{\gamma_s(m_j^{(2)} \tilde{K}_j)}{\gamma_s(m_j^{(2)} T_{j,*}^{(2)})} + \frac{\gamma_s(m_j^{(1)} (T_{j,*}^{(1)} \wedge T_{j,*}^{(2)})) - \gamma_s(m_j^{(1)} \tilde{K}_j)}{\gamma_s(m_j^{(1)} T_{j,*}^{(1)})} & \text{for } m_j^{(1)} > m_j^{(2)} \end{cases} \end{aligned}$$

for $m_{j,t}^{(i)} = \frac{\xi_t^{(i)}(\beta_{j,t}^{(i)})^2}{2(\sigma_t^{(i)})^2}$, $T_{j,*}^{(i)} := \frac{(U_{j,*}^{(i)})^{-\frac{2}{1+\nu}-1}}{\nu}$, $s = \frac{1+\nu}{2}$, $\gamma_s(x) = \frac{1}{\Gamma(s)} \int_0^x t^{s-1} e^{-t} dt \in [0, 1]$ the regularized incomplete lower Gamma function, $a \wedge b := \min\{a, b\}$, $a \vee b := \max\{a, b\}$, and

$$\tilde{K}_j := \left(0 \vee \left(\frac{\log \left(\left(\frac{m_j^{(2)}}{m_j^{(1)}} \right)^s \frac{\gamma_s(m_j^{(1)} T_{j,*}^{(1)})}{\gamma_s(m_j^{(2)} T_{j,*}^{(2)})} \right)}{m_j^{(2)} - m_j^{(1)}} \right) \right) \wedge (T_{j,*}^{(1)} \wedge T_{j,*}^{(2)}).$$

Proof. We work component-wise and drop the subscripts for ease of notation. Then for $i = 1, 2$, distributions $P^{(i)}$ has density

$$p(\eta; m^{(i)}, T^{(i)}) = \eta^{s-1} e^{-m^{(i)}\eta} \frac{(m^{(i)})^s}{\Gamma(s) \gamma_s(m^{(i)} T^{(i)})}$$

on $(0, T^{(i)})$ for $i = 1, 2$ respectively, where $T^{(i)} := \frac{(U_{j,*}^{(i)})^{-\frac{2}{1+\nu}-1}}{\nu}$, $s = \frac{1+\nu}{2}$ and $\gamma_s(x) = \frac{1}{\Gamma(s)} \int_0^x t^{s-1} e^{-t} dt \in [0, 1]$ is the regularized incomplete lower Gamma function. Note that

$$\mathbb{P}_{\max}\left(\eta^{(1)} = \eta^{(2)} \mid T^{(1)}, T^{(2)}, m^{(1)}, m^{(2)}\right) = \int_0^{T^{(1)} \wedge T^{(2)}} p(\eta; m^{(1)}, T^{(1)}) \wedge p(\eta; m^{(2)}, T^{(2)}) d\eta.$$

Case $m^{(1)} = m^{(1)}$.

$$\begin{aligned}
& \int_0^{T^{(1)} \wedge T^{(2)}} p(\eta; m^{(1)}, T^{(1)}) \wedge p(\eta; m^{(2)}, T^{(2)}) d\eta \\
&= \int_0^{T^{(1)} \wedge T^{(2)}} \eta^{s-1} \frac{(m^{(1)})^s}{\Gamma(s)} \left(\frac{1}{\gamma_s(m^{(1)}T^{(1)})} \wedge \frac{1}{\gamma_s(m^{(1)}T^{(2)})} \right) d\eta \\
&= \int_0^{T^{(1)} \wedge T^{(2)}} \eta^{s-1} \frac{(m^{(1)})^s}{\Gamma(s)} \frac{1}{\gamma_s(m^{(1)}(T^{(1)} \vee T^{(2)}))} \\
&= \frac{\gamma_s(m^{(1)}(T^{(1)} \wedge T^{(2)}))}{\gamma_s(m^{(1)}(T^{(1)} \vee T^{(2)}))}
\end{aligned}$$

as required.

Case $m^{(1)} < m^{(2)}$. For $0 < \eta \leq T^{(1)} \wedge T^{(2)}$,

$$\begin{aligned}
p(\eta; m^{(1)}, T^{(1)}) \leq p(\eta; m^{(2)}, T^{(2)}) &\Leftrightarrow \exp((m^{(2)} - m^{(1)})\eta) \leq \left(\frac{m^{(2)}}{m^{(1)}} \right)^s \frac{\gamma_s(m^{(1)}T^{(1)})}{\gamma_s(m^{(2)}T^{(2)})} \\
&\Leftrightarrow \eta \leq \frac{\log \left(\left(\frac{m^{(2)}}{m^{(1)}} \right)^s \frac{\gamma_s(m^{(1)}T^{(1)})}{\gamma_s(m^{(2)}T^{(2)})} \right)}{m^{(2)} - m^{(1)}} =: K.
\end{aligned}$$

Denote $\tilde{K} := (0 \vee K) \wedge (T^{(1)} \wedge T^{(2)})$, such that

$$\tilde{K} := \begin{cases} 0 & \text{when } K \leq 0 \\ K & \text{when } 0 < K \leq T^{(1)} \wedge T^{(2)} \\ T^{(1)} \wedge T^{(2)} & \text{when } T^{(1)} \wedge T^{(2)} < K. \end{cases}$$

This gives

$$\begin{aligned}
& \int_0^{T^{(1)} \wedge T^{(2)}} p(\eta; m^{(1)}, T^{(1)}) \wedge p(\eta; m^{(2)}, T^{(2)}) d\eta \\
&= \int_0^{\tilde{K}} p(\eta; m^{(1)}, T^{(1)}) d\eta + \int_{\tilde{K}}^{T^{(1)} \wedge T^{(2)}} p(\eta; m^{(2)}, T^{(2)}) d\eta \\
&= \left(\frac{\Gamma(s)\gamma_s(m^{(1)}\tilde{K})}{(m^{(1)})^s} \right) \left(\frac{(m^{(1)})^s}{\Gamma(s)\gamma_s(m^{(1)}T^{(1)})} \right) \\
&\quad + \left(\frac{\Gamma(s)(\gamma_s(m^{(2)}(T^{(1)} \wedge T^{(2)})) - \gamma_s(m^{(2)}\tilde{K}))}{(m^{(2)})^s} \right) \left(\frac{(m^{(2)})^s}{\Gamma(s)\gamma_s(m^{(2)}T^{(2)})} \right) \\
&= \frac{\gamma_s(m^{(1)}\tilde{K})}{\gamma_s(m^{(1)}T^{(1)})} + \frac{\gamma_s(m^{(2)}(T^{(1)} \wedge T^{(2)})) - \gamma_s(m^{(2)}\tilde{K})}{\gamma_s(m^{(2)}T^{(2)})}.
\end{aligned}$$

as required.

Case $m^{(1)} > m^{(2)}$. Follows from the $m^{(1)} < m^{(2)}$ case by symmetry. \square

C Additional Algorithms

Algorithm 7: Maximal coupling with independent residuals.

Input: Distributions P and Q with respective densities p and q

Sample $X \sim P$, and $W \sim \text{Uniform}(0, 1)$.

if $p(X)W \leq q(X)$ **then** set $Y = X$ and **return** (X, Y) .

else sample $\tilde{Y} \sim Q$ and $\tilde{W} \sim \text{Uniform}(0, 1)$ until $q(\tilde{Y})\tilde{W} > p(\tilde{Y})$. Set $Y = \tilde{Y}$ and **return** (X, Y) .

Algorithm 9: Fast Sampling of Normals for Gaussian scale mixture priors [Bhattacharya et al., 2016].

Result: Sample from $\mathcal{N}((X^T X + \xi Diag(\eta))^{-1} X^T y, \sigma^2 (X^T X + \xi Diag(\eta))^{-1})$

1. Sample $r \sim \mathcal{N}(0, I_p)$, $\delta \sim \mathcal{N}(0, I_n)$
2. Let $u = \frac{1}{\sqrt{\xi\eta}}r$, $v = Xu + \delta$. Calculate $v^* = M^{-1}(\frac{y}{\sigma} - v)$ for $M = I_n + (\xi)^{-1} X Diag(\eta^{-1}) X^T$. Let $U = (\xi\eta)^{-1} X^T$. Set $\beta = \sigma(u + Uv^*)$.

Algorithm 10: Coupled Normals for Gaussian scale mixture priors with common random numbers.

Input: $\eta_{t+1}^{(1)}, \xi_{t+1}^{(1)}, (\sigma_{t+1}^{(1)})^2, \eta_{t+1}^{(2)}, \xi_{t+1}^{(2)}, (\sigma_{t+1}^{(2)})^2$.

1. Sample $r \sim \mathcal{N}(0, I_p)$, $\delta \sim \mathcal{N}(0, I_n)$.
2. For $i = 1, 2$, let $u^{(i)} = \frac{1}{\sqrt{\xi_{t+1}^{(i)} \eta_{t+1}^{(i)}}}r$, $v^{(i)} = Xu^{(i)} + \delta$. Calculate $v^{(i),*} = M_{\xi_{t+1}^{(i)}, \eta_{t+1}^{(i)}}^{-1}(\frac{y}{\sigma_{t+1}^{(i)}} - v)$ for $M_{\xi_{t+1}^{(i)}, \eta_{t+1}^{(i)}} = I_n + (\xi_{t+1}^{(i)})^{-1} X Diag(\eta_{t+1}^{(i)})^{-1} X^T$. Let $U^{(i)} = (\xi_{t+1}^{(i)} \eta_{t+1}^{(i)})^{-1} X^T$. Set $\beta_{t+1}^{(i)} = \sigma_{t+1}^{(i)}(u^{(i)} + U^{(i)}v^{(i),*})$.

return $(\beta_{t+1}^{(1)}, \beta_{t+1}^{(2)})$

Algorithm 11: Coupled Metropolis–Hastings for $\xi|\eta$ updates with exact meetings.

Input: $\xi_t^{(1)}, \xi_t^{(2)} > 0$ and $\eta_{t+1}^{(1)}, \eta_{t+1}^{(2)} \in \mathbb{R}_{>0}^p$.
Sample joint proposal

$$\left(\log(\xi^{*,(1)}), \log(\xi^{*,(2)}) \right) \Big| \xi_t^{(1)}, \xi_t^{(2)} \sim \gamma_{max} \left(\mathcal{N}(\log(\xi_t^{(1)}), \sigma_{\text{MH}}^2), \mathcal{N}(\log(\xi_t^{(2)}), \sigma_{\text{MH}}^2) \right).$$

where σ_{MH} is the Metropolis–Hastings step-size, and γ_{max} is a maximal coupling with independent residuals (Algorithm 7).

For $i = 1, 2$, calculate log-acceptance probability

$$\log(q^{(i)}) = \log \left(\frac{L(y|\xi^{*,(i)}, \eta_{t+1}^{(i)}) \pi_\xi(\xi^{*,(i)})}{L(y|\xi_t^{(i)}, \eta_{t+1}^{(i)}) \pi_\xi(\xi_t^{(i)})} \frac{\xi^{*,(i)}}{\xi_t^{(i)}} \right),$$

with log-likelihood $\log(L(y|\xi, \eta))$ as defined in Algorithm 1 Equation (6).

Sample $U^* \sim \text{Uniform}(0, 1)$.

if $U^* \leq q^{(1)}$ **then** set $\xi_{t+1}^{(1)} := \xi^{*,(1)}$ **else** set $\xi_{t+1}^{(1)} := \xi_t^{(1)}$.
if $U^* \leq q^{(2)}$ **then** set $\xi_{t+1}^{(2)} := \xi^{*,(2)}$ **else** set $\xi_{t+1}^{(2)} := \xi_t^{(2)}$.
return $(\xi_{t+1}^{(1)}, \xi_{t+1}^{(2)})$.

Algorithm 12: Perfect sampling of $\xi|\eta$.

Input: $\nu \in \mathbb{R}_{>0}^p$, discretized grid G on the compact support of $\pi_\xi(\cdot)$

Perform eigenvalue decomposition $X Diag(\eta)^{-1} X^T = Q \Lambda Q^T$ for orthogonal matrix Q and diagonal matrix Λ .

Calculate unnormalized probability mass function

$$\widetilde{pmf}(\xi|\eta) := \left(\prod_{i=1}^n (1 + \xi^{-1} \Lambda_{i,i}) \right)^{-1/2} \left(b_0 + \sum_{i=1}^n [Qy]_i^2 \frac{1}{1 + \xi^{-1} \Lambda_{i,i}} \right)^{-\frac{a_0+n}{2}} \pi_\xi(\xi)$$

for each $\xi \in G$, where $[Qy]_i$ is the i^{th} entry of $Qy \in \mathbb{R}^n$.

Normalize to obtain probability mass function: $pmf(\xi|\eta) = \frac{\widetilde{pmf}(\xi|\eta)}{\sum_{\xi \in G} \widetilde{pmf}(\xi|\eta)}$.

Sample $\xi \sim pmf(\cdot|\eta)$ on G using probability inverse transform.

return ξ .

Algorithm 13: Perfect sampling of $\eta_j|\beta_j, \sigma^2, \xi$.

Input: $\nu, m_j := \frac{\xi \beta_j^2}{2\sigma^2} > 0$.

Sample $W^* \sim \text{Uniform}(0, 1)$

Set

$$\eta_j = \frac{1}{\nu} U_{\frac{\nu+1}{2}, 1, \frac{m_j}{\nu}}^{-1} \left(W^* U_{\frac{\nu+1}{2}, 1, \frac{m_j}{\nu}}(\infty) \right) \quad (43)$$

where $U_{a,b,z}(t) := \frac{1}{\Gamma(a)} \int_0^t x^{a-1} (1+x)^{b-a-1} e^{-zx} dx$ is defined as the *lower incomplete* confluent hypergeometric function of the second kind, such that $U_{a,b,z}(\infty) = U(a, b, z)$ gives the confluent hypergeometric function of the second kind.

return η_j .

D Algorithm Derivations

Gibbs sampler for Half- $t(\nu)$ priors (Algorithm 1). Derivation of the blocked Gibbs sampling algorithm (Algorithm 1) is given in [Johndrow et al. \[2020\]](#) for the Horseshoe prior. For Half- $t(\nu)$ priors, it remains to check the validity of the slice sampler in Algorithm 2. Working component-wise, let $p(\eta|m)$ denote the conditional density of η given $m > 0$. Then,

$$p(\eta|m) \propto \eta^{\frac{\nu-1}{2}} (1 + \nu\eta)^{-\frac{1+\nu}{2}} e^{-m\eta} \mathbb{1}_{(0,\infty)}(\eta) = \int_{u=0}^{\infty} \eta^{\frac{\nu-1}{2}} e^{-m\eta} \mathbb{1}_{(0,\infty)}(\eta) \mathbb{1}_{(0,(1+\nu\eta)^{-\frac{1+\nu}{2}})}(u) du.$$

Let $\bar{p}(\eta, u|m) \propto \eta^{\frac{\nu-1}{2}} e^{-m\eta} \mathbb{1}_{(0,\infty)}(\eta) \mathbb{1}_{(0,(1+\nu\eta)^{-\frac{1+\nu}{2}})}(u)$ be the conditional density of the augmented random variable (η, u) given m , such that $p(\eta|m) = \int_{u=0}^{\infty} \bar{p}(\eta, u|m) du$. Then, the slice sampler in Algorithm 2 corresponds to a Gibbs sampler targeting $\bar{p}(\eta, u|m)$:

$$\begin{aligned} \bar{p}(u|\eta, m) &\sim \text{Uniform}\left(0, (1 + \nu\eta)^{-\frac{1+\nu}{2}}\right), \\ \bar{p}(\eta|u, m) &\propto \eta^{\frac{\nu-1}{2}} e^{-m\eta} \mathbb{1}_{(0, \frac{u^{-2/(1+\nu)} - 1}{\nu})}(\eta). \end{aligned}$$

Note that $\int_0^x \eta^{s-1} e^{-m\eta} d\eta = m^{-s} \Gamma(s) \gamma_s(mx)$, where $\gamma_s(x) := \frac{1}{\Gamma(s)} \int_0^x t^{s-1} e^{-t} dt \in [0, 1]$ is the regularized incomplete lower Gamma function. For $T = (u^{-2/(1+\nu)} - 1)/\nu$, $s = \frac{1+\nu}{2}$, we can now obtain the cumulative density function of $\bar{p}(\cdot|u, m)$, given by $\int_0^x \bar{p}(\eta|u, m) = \gamma_s(mx)/\gamma_s(mT)$ for $0 \leq x \leq T$. By probability inverse transform, we can now sample perfectly from $\eta|u, m$, such that

$$\eta := \frac{1}{m} \gamma_s^{-1}(\gamma_s(mT)U^*) \text{ for } U^* \sim \text{Uniform}(0, 1)$$

as in Step (2) of Algorithm 2.

Perfect sampling of $\xi|\eta$ (Algorithm 12). In Algorithm 1, we have

$$p(\xi|\eta) \propto |M_{\xi,\eta}|^{-1/2} (b_0 + y^T M_{\xi,\eta}^{-1} y)^{-\frac{a_0+n}{2}} \pi_{\xi}(\eta)$$

for $M_{\xi,\eta} = I_n + \xi^{-1} X Diag(\eta)^{-1} X^T$ and $\pi_{\xi}(\cdot)$ the prior density on ξ . Consider the eigenvalue decomposition of $X Diag(\eta)^{-1} X^T$, such that $X Diag(\eta)^{-1} X^T = Q \Lambda Q^T$ for Q orthogonal and Λ diagonal. Then,

$$\begin{aligned} |M_{\xi,\eta}| &= |Q(I_n + \xi^{-1} \Lambda)Q^T| = |I_n + \xi^{-1} \Lambda| = \prod_{i=1}^n (1 + \xi^{-1} \Lambda_{i,i}) \\ y^T M_{\xi,\eta}^{-1} y &= y^T Q(I_n + \xi^{-1} \Lambda)^{-1} Q^T y = \sum_{i=1}^n [Q^T y]_i^2 (1 + \xi^{-1} \Lambda_{i,i})^{-1} \end{aligned}$$

This allows the discretized perfect sampling of ξ given η using probability inverse transform as in Algorithm 12, with $\mathcal{O}(n^3)$ computational cost arising from eigenvalue decomposition of $X Diag(\eta)^{-1} X^T$.

Perfect sampling of $\eta_j|\beta_j, \sigma^2, \xi$ (Algorithm 13). Working component-wise, let

$$p(\eta|m) \propto \eta^{\frac{\nu-1}{2}} (1 + \nu\eta)^{-\frac{1+\nu}{2}} e^{-m\eta}$$

denote the conditional density of $\eta \in (0, \infty)$ given $m > 0$. We can calculate the corresponding cumulative density function (see proof of Proposition B.1), given by

$$\int_0^K p(\eta|m) d\eta = \frac{U_{\frac{\nu+1}{2}, 1, \frac{m}{\nu}}(\nu K)}{U(\frac{\nu+1}{2}, 1, \frac{m}{\nu})}.$$

where $U_{a,b,z}(t) := \frac{1}{\Gamma(a)} \int_0^t x^{a-1} (1+x)^{b-a-1} e^{-zx} dx$ is defined as the *lower incomplete confluent hypergeometric function of the second kind*. Algorithm 13 and Equation (43) directly follow from probability inverse transform.